ISSN 0915-633X

NATIONAL INSTITUTE FOR FUSION SCIENCE

CTBC
A Program to Solve the Collinear Three-Body Coulomb Problem: Bound States and Scattering Below the Three-Body Disintegration Threshold

Oleg I. Tolstikhin and C. Namba

(Received - June 9, 2003)

NIFS-779 Aug. 2003

This report was prepared as a preprint of work performed as a collaboration research of the National Institute for Fusion Science (NIFS) of Japan. The views presented here are solely those of the authors. This document is intended for information only and may be published in a journal after some rearrangement of its contents in the future.

Inquiries about copyright should be addressed to the Research Information Center, National Insitute for Fusion Science, Oroshi-cho, Toki-shi, Gifu-ken 509-5292 Japan.

E-mail: bunken@nifs.ac.jp

<Notice about photocopying>

In order to photocopy any work from this publication, you or your organization must obtain permission from the following organizaion which has been delegated for copyright for clearance by the copyright owner of this publication.

Except in the USA

Japan Academic Association for Copyright Clearance (JAACC)
41-6 Akasaka 9-chome, Minato-ku, Tokyo 107-0052 Japan
TEL:81-3-3475-5618 FAX:81-3-3475-5619 E-mail:naka-atsu@muj.biglobe.ne.jp

In the USA

Copyright Clearance Center, Inc.
222 Rosewood Drive, Danvers, MA 01923 USA
Phone: (978) 750-8400 FAX: (978) 750-4744

TOKI, JAPAN

CTBC

A Program to Solve the Collinear Three-Body Coulomb Problem: Bound States and Scattering Below the Three-Body Disintegration Threshold

Oleg I. Tolstikhin

Russian Research Center "Kurchatov Institute"

Kurchatov Square 1, Moscow 123182, Russia

olegit@imp.kiae.ru

Chusei Namba

National Institute for Fusion Science

Toki, 509-5292, Japan

Abstract

A program to solve the quantum-mechanical collinear three-body Coulomb problem is described and illustrated by calculations for a number of representative systems and processes. In the internal region, the Schrödinger equation is solved in hyperspherical coordinates using the slow/smooth variable discretization method. In asymptotic regions, the solution is obtained in Jacobi coordinates using the asymptotic package GAILIT from the CPC library. Only bound states and scattering processes below the three-body disintegration threshold are considered here; resonances and fragmentation processes will be discussed in subsequent parts of this series.

Keywords: three-body Coulomb problem, bound states, scattering matrix, hyperspherical adiabatic approach, slow/smooth variable discretization method, discrete variable representation

Contents

I. Introduction 4

II. Basic equations 5

A. Description of the system and formulation of the problem 5

B. Schrödinger equation in a laboratory frame 7

C. Separation of the motion of the center of mass 9

D. Jacobi coordinates 10

E. Hyperspherical coordinates 12

F. Scaling 13

G. Permutation symmetry in the symmetric case 15

H. Asymptotic states 16

I. Asymptotic boundary conditions 17

III. Hyperspherical adiabatic (HSA) approach 19

A. HSA eigenvalue problem 19

B. HSA expansion 20

IV. Slow/smooth variable discretization (SVD) method 22

A. SVD eigenvalue problem 22

B. SVD solution 24

V. Numerical procedure 25

A. Solution of HSA eigenvalue problem 25

B. Bound state calculations 26

C. Scattering calculations 27

1. Internal region 28

2. Asymptotic regions 30

3. Matching 32

D. Structure of the program 33

VI. Illustrative calculations 34

A. *epe*, $\sigma = +$ (case A) 35

B. epe, $\sigma = -$ (case A) 36
C. pee (case B) 37
D. ee^+e, $\sigma = +$ (case A) 38
E. ee^+e, $\sigma = -$ (case A) 39
F. e^+ee (case B) 40
G. pee^+ (case A) 41
H. epe^+ (case B1) 43
I. ee^+p (case B2) 44
J. $t\mu d$ (case A) 45

VII. Conclusions 47

Acknowledgments 47

A. Asymptotic states 48
1. Bound-motion part 48
a. Hydrogenic states 48
b. Hydrogenic states in a box 49
2. Free-motion part 51
a. Coulomb wave 51
b. Multichannel Coulomb wave with multipole couplings 52

B. Discrete variable representations (DVR) based on classical orthogonal polynomials (COP) 53
1. DVR basis 53
2. Application of DVR to the solution of a Sturm-Liouville problem 56
3. Application of DVR in the SVD method 60
a. Kinetic matrix for bound states 60
b. Kinetic matrix for scattering in the first sector 60
c. Kinetic matrix for scattering in further sectors 61
d. Weight matrix 62

References 64

I. INTRODUCTION

It is well known that the two-body Coulomb problem (the theory of hydrogen-like atoms) allows a complete analytical solution. It will not be an exaggeration to say that this solution provides a foundation for the whole field of atomic physics. The three-body Coulomb problem (the theory of two-electron atoms, one-electron diatomic molecules, and more exotic systems which apart from nuclei and electrons include also positrons, muons and other elementary particles) is the next problem in terms of the number of particles involved. It is much richer in contents, in fact it is the simplest (but far nontrivial) realistic model which embraces *all* types of phenomena (bound states, resonances, elastic scattering, excitation, rearrangement, and fragmentation processes) considered in the theory of atomic and molecular collisions. This problem is not solvable analytically, but it is still simple enough to be studied by exact (analytical and numerical) methods, i.e., beyond any approximations. The results of such studies, besides being interesting in themselves, may shed a new light on the behavior of more complex systems.

This work is a part of a larger project whose goal is to comprehend major mechanisms governing the quantum dynamics of three-body Coulomb systems via the synergism of asymptotic methods and modern computer resources and computational technologies. Here we consider the three-body Coulomb problem in one-dimensional world — the so-called collinear three-body Coulomb problem. This simplified problem allows a relatively cheap in terms of computational expenses required and very accurate numerical solution and at the same time preserves basic features that make the dynamics of the full-scale three-dimensional three-body Coulomb problem so nontrivial, thus presenting an excellent model for studying the dynamics. In this work we describe a program CTBC which enables one to solve the collinear three-body Coulomb problem numerically and illustrate its application by calculations for a number of representative systems and processes. Such quantitative analysis is essential as a source of information using which a qualitative understanding will hopefully be developed in future studies.

This work is written with the intention to make it self-contained and understandable to a student. All necessary technical details are given in the main text or in appendices. We hope it will be useful for students who wish to continue our efforts as an introduction into the field, but also for all interested physicists who wish to use program CTBC.

II. BASIC EQUATIONS

A. Description of the system and formulation of the problem

We consider a system of three particles restricted to move along a straight line and interacting via the Coulomb forces. It is assumed that particles cannot penetrate through each other in collisions, so they preserve their order on the line. In fact, this is not an assumption but a consequence of the dimension of the problem; we shall return to this point in the discussion of boundary conditions. Particles are enumerated and will be called by their numbers $i = 1, 2, 3$, and pairs of particles will be called by the number of the remaining particle. It is more convenient to have natural order of pairs rather than of particles, therefore particles are numbered as shown in Fig. 1a. Then only pairs 1 and 2 can be formed when the system disintegrates into a free particle and a bound pair. Particles are assumed to be structureless and completely characterized by their masses m_i and charges e_i;

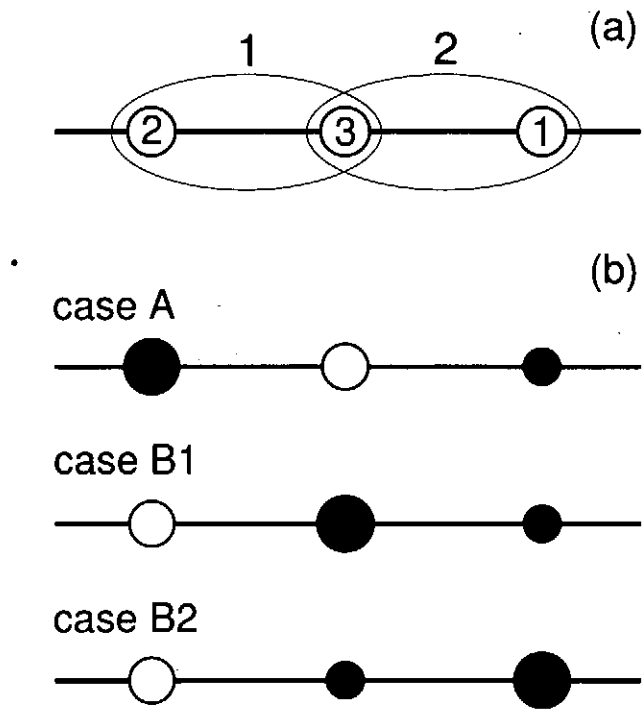

FIG. 1: Three particles on a line. (a) The convention for their numbers; this order does not change during the motion. (b) Three physically different variants of their relative position; open circles — the oppositely charged particle, solid circles — similarly charged particles, the difference in their size symbolizes a difference between the particles.

two particles with equal masses and charges will be treated as identical. We shall consider only the case when one of the particles is charged oppositely to the others. Then two of three interparticle interactions are attractive and one is repulsive, pairs of particles can form bound states, and there is a rich variety of scattering processes that can occur in the system. The other possibility, i.e., when all three particles are charged similarly, is of less interest from the physical viewpoint. By convention we assume that $e_2e_3 < 0$, i.e., the interaction in pair 1 is attractive. Then there are two possibilities: either $e_1e_3 < 0$ or $e_1e_3 > 0$, which will be referred to as cases A and B, respectively. In case A, the oppositely charged particle has number 3, see Fig. 1b. Interchanging similarly charged particles 1 and 2 in this case does not lead to a new physical situation, because it can be compensated by changing the direction of the variation of a coordinate on the line. So the way of numbering similarly charged particles in the case A is a matter of convention which will be specified later. Case A under an additional condition that particles 1 and 2 are identical will be called the symmetric case. In case B, the oppositely charged particle has number 2. Now interchanging similarly charged particles 3 and 1 does lead to a new physical situation, if these particles are not identical. Accordingly, we shall distinguish two subcases, B1 and B2, illustrated in Fig. 1b; their formal definition will also be given later. Cases A, B1, and B2 exhaust all physically different variants of the relative position of three given particles on the line.

Considering evolution of this system in time, its initial and final states can be classified by the number of fragments. There are three types of states: (i) one fragment, i.e., bound states of the whole system, (ii) two fragments, i.e., a free particle and a bound pair, and (iii) three fragments, i.e., three free particles. In case A, the system can disintegrate into two fragments in two ways, (23) + 1 and 2 + (31), which will be called arrangements 1 and 2, respectively, while in case B such disintegration may occur only in the arrangement 1. The same classification applies to initial and final states of scattering processes in time-independent formulation which will be used in this work. Thus, depending on its energy, the system can be found in one of the following (bound or scattering) stationary states:
in both cases A and B

$$(231) \qquad \text{— bound (ground and excited) states,} \qquad (1a)$$

$$\langle 231 \rangle \qquad \text{— resonance (complex energy) states,} \qquad (1b)$$

$(23)_i + 1 \to (23)_f + 1$ — elastic scattering and excitation in the arrangement 1, (1c)

$(23)_i + 1 \to 2 + 3 + 1$ — fragmentation in the arrangement 1, (1d)

and in addition in case A only

$2 + (31)_i \to 2 + (31)_f$ — elastic scattering and excitation in the arrangement 2, (1e)

$\left.\begin{array}{l}(23)_i + 1 \to 2 + (31)_f \\ 2 + (31)_i \to (23)_f + 1\end{array}\right\}$ — rearrangement, (1f)

$2 + (31)_i \to 2 + 3 + 1$ — fragmentation in the arrangement 2, (1g)

where indices i and f identify states of the bound pair in the initial and final states of the system, respectively. The purpose of program CTBC is to provide an accurate numerical description of all these states in a wide interval of energy for arbitrary combinations of the masses and charges of particles. In this work we consider only bound states (1a) and scattering processes (1c), (1e), and (1f) below the threshold of fragmentation processes (1d) and (1g). Resonances (1b) and scattering processes (1c)-(1g) above this threshold will be discussed in subsequent parts of this series.

B. Schrödinger equation in a laboratory frame

Let us introduce a coordinate X on the line with the origin at the position of an unmovable observer (a laboratory), and let X_i be the coordinates of particles, see Fig. 2a. The Schrödinger equation in these coordinates reads

$$(\mathcal{T} + V - \mathcal{E})\Psi(X_1, X_2, X_3) = 0, \tag{2}$$

where $\mathcal{T}$ is the kinetic energy,

$$\mathcal{T} = -\frac{1}{2m_1}\frac{\partial^2}{\partial X_1^2} - \frac{1}{2m_2}\frac{\partial^2}{\partial X_2^2} - \frac{1}{2m_3}\frac{\partial^2}{\partial X_3^2}, \tag{3}$$

V is the Coulomb potential energy,

$$V = \frac{e_2 e_3}{|X_2 - X_3|} + \frac{e_3 e_1}{|X_3 - X_1|} + \frac{e_1 e_2}{|X_1 - X_2|}, \tag{4}$$

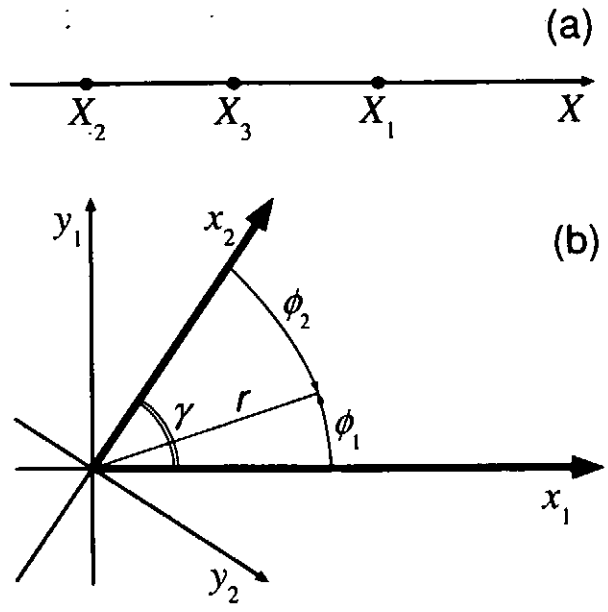

FIG. 2: Different sets of coordinates used in the problem. (a) Individual particles' coordinates X_i defining a three-dimensional configuration space of the system $\mathbb{R}^3$. (b) Jacobi (x_α, y_α) and hyperspherical (r, ϕ_α) coordinates in the reduced configuration space $\mathbb{R}^2$. Only the sector lying between two thick lines is considered; the wave function vanishes along these lines.

and $\mathcal{E}$ is the total energy of the system. Configuration space can be thought of as a three-dimensional Euclidean space $\mathbb{R}^3$ with Cartesian coordinates (X_1, X_2, X_3). Interparticle collisions occur on the planes $X_1 = X_2$, $X_2 = X_3$, and $X_3 = X_1$ which intersect each other along the line of triple collisions $X_1 = X_2 = X_3$, dividing the configuration space into sectors. In order that matrix elements of the potential energy (4) be finite, the solutions of Eq. (2) must vanish on these planes. This requirement is a mathematical formulation of the mentioned above physical condition that particles cannot penetrate through each other; it is specific to one-dimensional Coulomb problems, the situation in spaces of higher dimension is different. Thus Eq. (2) can be considered separately in each sector, and by interchanging particles the problem can be reduced to the consideration of one particular sector. Assuming that particles are in the order shown in Fig. 2a, the coordinates X_i are restricted to vary in the sector

$$-\infty < X_2 \leq X_3 \leq X_1 < \infty, \tag{5}$$

and the wave function must vanish on its boundaries,

$$\Psi(X_1, X_2, X_3)|_{X_2=X_3} = \Psi(X_1, X_2, X_3)|_{X_3=X_1} = 0. \tag{6}$$

Only this sector will be considered in the following. Inside it, we can rewrite Eq. (4) as

$$V = \frac{e_2 e_3}{X_3 - X_2} + \frac{e_3 e_1}{X_1 - X_3} + \frac{e_1 e_2}{X_1 - X_2}. \tag{7}$$

C. Separation of the motion of the center of mass

The center of mass of the system is located at

$$X_{\rm cm} = \frac{1}{M}\,(m_1 X_1 + m_2 X_2 + m_3 X_3), \tag{8}$$

where

$$M = m_1 + m_2 + m_3. \tag{9}$$

Let $\mathbf{r}$ denote a set of two variables defining the positions of particles for a given value of $X_{\rm cm}$; a two-dimensional Euclidean space $\mathbb{R}^2$ spanned by $\mathbf{r}$ will be called the reduced configuration space. We wish to change independent variables in Eq. (2) from (X_1, X_2, X_3) to $(X_{\rm cm}, \mathbf{r})$. This can be partially done without specifying $\mathbf{r}$. Indeed, variations of $X_{\rm cm}$ without changing $\mathbf{r}$ correspond to motions parallel to the line $X_1 = X_2 = X_3$, and variations of $\mathbf{r}$ without changing $X_{\rm cm}$ correspond to motions parallel to the plane $X_{\rm cm} = 0$. Let us introduce mass-scaled coordinates $X_i' = \sqrt{m_i}\,X_i$ in $\mathbb{R}^3$. After such scaling, the line $X_1 = X_2 = X_3$ and the plane $X_{\rm cm} = 0$ become orthogonal. The kinetic energy operator (3) reduces to a three-dimensional Laplacian in terms of X_i'. Its transformation to coordinates $(X_{\rm cm}, \mathbf{r})$ can be performed by a rotation of the frame (X_1', X_2', X_3') which brings one of its axes into the position of the line $X_1 = X_2 = X_3$, and then the other two will lie in the plane $X_{\rm cm} = 0$. Because the Laplacian preserves its form under rotations, there will be no cross derivatives in the expression for $\mathcal{T}$ in terms of the new variables, and hence no cross derivatives with respect to $X_{\rm cm}$ and $\mathbf{r}$. Knowing this, it can be shown that

$$\mathcal{T} = -\frac{1}{2M}\,\frac{\partial^2}{\partial X_{\rm cm}^2} + T, \tag{10}$$

where the reduced kinetic energy T is a differential operator acting on the variables $\mathbf{r}$ only. The potential energy (7) depends only on the distances between particles which are determined by $\mathbf{r}$. Thus we can separate variables $X_{\rm cm}$ and $\mathbf{r}$ in Eq. (2). Substituting into Eq. (2)

$$\Psi(X_1, X_2, X_3) = \exp(iK_{\rm cm} X_{\rm cm})\Psi(\mathbf{r}) \tag{11}$$

and

$$\mathcal{E} = \frac{K_{\rm cm}^2}{2M} + E, \tag{12}$$

where $K_{\rm cm}$ is the momentum corresponding to the motion in $X_{\rm cm}$ and E is the reduced energy of the system (its energy in the center-of-mass frame), we obtain a two-dimensional differential equation describing dynamics in the reduced configuration space

$$(T + V - E)\Psi(\mathbf{r}) = 0. \tag{13}$$

Only this equation will be considered in the following, so we shall refer to T and E simply as the kinetic and total energy of the system, omitting the adjective 'reduced'. When particles are at rest ($T = 0$) at infinite distances from each other ($V = 0$) we have $E = 0$, which defines the three-body disintegration threshold energy. In this work we consider only the solutions of Eq. (13) for $E < 0$. Because the solutions will be expressed in terms of different sets of coordinates in the different parts of configuration space, in some situations it will be convenient to leave coordinates unspecified. In such cases, we shall use notation $\mathbf{r}$ for the argument of the wave function.

D. Jacobi coordinates

Let us introduce reduced masses

$$\mu_i = \frac{m_{i+1} m_{i+2}}{m_{i+1} + m_{i+2}} \tag{14}$$

and angles of kinematic rotations

$$\gamma_i = \arctan \sqrt{\frac{m_i M}{m_{i+1} m_{i+2}}}, \quad 0 \le \gamma_i \le \pi/2, \tag{15}$$

where $(i, i+1, i+2)$ is a cyclic permutation of $(1, 2, 3)$. The angles γ_i satisfy

$$\gamma_1 + \gamma_2 + \gamma_3 = \pi. \tag{16}$$

We shall also use the simplified notation $\gamma \equiv \gamma_3$. In addition, it is convenient to introduce the parameter

$$\varepsilon = \frac{\gamma_2 - \gamma_1}{\gamma_3}, \quad -1 \le \varepsilon \le 1, \tag{17}$$

which characterizes mass-asymmetry of particles 1 and 2. In terms of γ and ε we have

$$\gamma_1 = \tfrac{1}{2}\,[\pi - (1+\varepsilon)\gamma], \tag{18a}$$

$$\gamma_2 = \tfrac{1}{2}\,[\pi - (1-\varepsilon)\gamma], \tag{18b}$$

and

$$\frac{m_1}{m_3} = \cot\gamma\,\cot[(1+\varepsilon)\gamma/2], \tag{19a}$$

$$\frac{m_2}{m_3} = \cot\gamma\,\cot[(1-\varepsilon)\gamma/2]. \tag{19b}$$

Jacobi coordinates are Cartesian coordinates in the reduced configuration space $\mathbb{R}^2$. There are infinitely many ways to introduce Jacobi coordinates, the different sets being related to each other by (kinematic) rotations and/or reflections. We shall use two particular sets of (mass-scaled) Jacobi coordinates defined by

$$\begin{aligned} x_1 &= \sqrt{\frac{m_1 m_2 m_3}{\mu_1 M}}\left(X_1 - \frac{m_2 X_2 + m_3 X_3}{m_2 + m_3}\right), \\ y_1 &= \sqrt{\mu_1}\,(X_3 - X_2), \end{aligned} \tag{20a}$$

and

$$\begin{aligned} x_2 &= \sqrt{\frac{m_1 m_2 m_3}{\mu_2 M}}\left(\frac{m_3 X_3 + m_1 X_1}{m_3 + m_1} - X_2\right), \\ y_2 &= \sqrt{\mu_2}\,(X_1 - X_3). \end{aligned} \tag{20b}$$

These coordinate systems are shown in Fig. 2b. They are related by

$$\begin{pmatrix} x_2 \\ y_2 \end{pmatrix} = \begin{pmatrix} \cos\gamma & \sin\gamma \\ \sin\gamma & -\cos\gamma \end{pmatrix} \begin{pmatrix} x_1 \\ y_1 \end{pmatrix}. \tag{21}$$

Jacobi coordinates of the 1st and 2nd sets are convenient for solving Eq. (13) in the asymptotic regions corresponding to disintegration of the system into two fragments in arrangements 1 and 2, respectively. In the following, arrangements will be specified by the Greek index α taking the values 1 or 2 in case A and only 1 in case B, and all the quantities relevant to the given arrangement will be indicated by the same subscript, e.g. (x_α, y_α). Many of equations below have identical forms for both arrangements; in such cases, we shall omit the subscript α where this does not lead to ambiguities. Substituting Eqs. (8) and (20) into Eq. (3) and comparing with Eq. (10) we obtain

$$T = -\frac{1}{2}\frac{\partial^2}{\partial x^2} - \frac{1}{2}\frac{\partial^2}{\partial y^2}. \tag{22}$$

The potential energy (7) as a function of Jacobi coordinates is given by

$$V = \frac{z_1}{y_1} + \frac{z_2}{x_1 \sin\gamma_3 - y_1 \cos\gamma_3} + \frac{z_3}{x_1 \sin\gamma_2 + y_1 \cos\gamma_2}, \tag{23a}$$

$$= \frac{z_1}{x_2 \sin\gamma_3 - y_2 \cos\gamma_3} + \frac{z_2}{y_2} + \frac{z_3}{x_2 \sin\gamma_1 + y_2 \cos\gamma_1}, \tag{23b}$$

where z_i are the pair charges,

$$z_i = e_{i+1} e_{i+2} \sqrt{\mu_i}. \tag{24}$$

As follows from Eqs. (5) and (6), the Schrödinger equation (13) must be solved in the sector

$$0 \le x < +\infty, \quad 0 \le y \le x \tan\gamma, \tag{25}$$

with the boundary conditions

$$\Psi(x,y)|_{y=0} = \Psi(x,y)|_{y=x\tan\gamma} = 0. \tag{26}$$

The volume element in $\mathbb{R}^2$ is given in terms of Jacobi coordinates by

$$d\mathcal{V} = dxdy. \tag{27}$$

E. Hyperspherical coordinates

Hyperspherical coordinates are polar coordinates in the reduced configuration space $\mathbb{R}^2$. They will be used for solving Eq. (13) in the internal region, where all three particles strongly interact with each other. We introduce two sets of hyperspherical coordinates, (r_1, ϕ_1) and (r_2, ϕ_2), defined in terms of the corresponding sets of Jacobi coordinates by

$$\begin{aligned} x &= r\cos\phi, \\ y &= r\sin\phi, \end{aligned} \quad \leftrightarrow \quad \begin{aligned} r &= \sqrt{x^2 + x^2}, \\ \phi &= \arctan(y/x). \end{aligned} \tag{28}$$

These coordinate systems are shown in Fig. 2b. Using Eq. (21), it can be shown that $r_1 = r_2$ and

$$\phi_1 + \phi_2 = \gamma. \tag{29}$$

The kinetic (22) and potential (23) energies in terms of hyperspherical coordinates read

$$T = -\frac{1}{2r}\frac{\partial}{\partial r} r \frac{\partial}{\partial r} - \frac{1}{2r^2}\frac{\partial^2}{\partial \phi^2} \tag{30}$$

and

$$V = \frac{1}{r}\left(\frac{z_1}{\sin\phi_1} + \frac{z_2}{\sin(\gamma_3-\phi_1)} + \frac{z_3}{\sin(\gamma_2+\phi_1)}\right), \tag{31a}$$

$$= \frac{1}{r}\left(\frac{z_1}{\sin(\gamma_3-\phi_2)} + \frac{z_2}{\sin\phi_2} + \frac{z_3}{\sin(\gamma_1+\phi_2)}\right). \tag{31b}$$

The sector (25) corresponds to

$$0 \le r < \infty, \quad 0 \le \phi \le \gamma, \tag{32}$$

the boundary conditions (26) take the form

$$\Psi(r,\phi)|_{\phi=0} = \Psi(r,\phi)|_{\phi=\gamma} = 0, \tag{33}$$

and the volume element (27) becomes

$$d\mathcal{V} = r dr d\phi. \tag{34}$$

As $r \to 0$, terms T, V, and E in Eq. (13) grow as r^{-2}, r^{-1}, and r^0, respectively, see Eqs. (30) and (31). Neglecting V and E, it can be shown that a general solution to Eqs. (13) and (33) behaves as

$$\Psi(r,\phi)|_{r\to 0} \propto r^{\pi/\gamma}\sin(\pi\phi/\gamma). \tag{35}$$

F. Scaling

We are going to consider systems with vastly different masses m_i and charges e_i of particles. In order to bring them to a common scale, it is convenient to introduce scaled coordinates

$$(\tilde{x},\tilde{y},\tilde{r}) \equiv h|z_1| \times (x,y,r), \qquad \tilde{\phi} \equiv h^{-1}\phi, \tag{36a}$$

scaled energies

$$(\tilde{T},\tilde{V},\tilde{E}) \equiv |z_1|^{-2} \times (T,V,E), \tag{36b}$$

and scaled charges

$$\tilde{z}_i \equiv |z_1|^{-1} \times z_i, \tag{36c}$$

where

$$h = \frac{2\gamma}{\pi}, \qquad 0 \le h \le 1. \tag{37}$$

Besides convenience in calculations, such scaling pursues a deeper goal: it reveals the parameter h (a resemblance of this notation to Planck's constant is not accidental) essential for the analysis of this problem by asymptotic methods (to be discussed in future publications). Only scaled quantities will be used in the following, so from here on we shall omit the tilde. After scaling, pair charges are explicitly given by

$$z_1 = -1, \tag{38a}$$

$$z_2 = -\frac{e_1}{e_2}\sqrt{\frac{m_1(m_2+m_3)}{m_2(m_1+m_3)}} = -\frac{e_1}{e_2}\frac{\cos[(1+\varepsilon)\gamma/2]}{\cos[(1-\varepsilon)\gamma/2]}, \tag{38b}$$

$$z_3 = -\frac{e_1}{e_3}\sqrt{\frac{m_1(m_3+m_2)}{m_3(m_1+m_2)}} = -\frac{e_1}{e_3}\sqrt{\frac{\cos\gamma+\cos\varepsilon\gamma}{2\sin^2\gamma}\frac{\cos[(1+\varepsilon)\gamma/2]}{\cos[(1-\varepsilon)\gamma/2]}}. \tag{38c}$$

Other changes in the above equations are summarized below.

Jacobi coordinates. The two sets (x_1, y_1) and (x_2, y_2) are related by the same equation (21). The kinetic (22) and potential (23) energies become

$$T = -\frac{h^2}{2}\frac{\partial^2}{\partial x^2} - \frac{h^2}{2}\frac{\partial^2}{\partial y^2} \tag{39}$$

and

$$V = \frac{hz_1}{y_1} + \frac{hz_2}{x_1\sin\gamma_3 - y_1\cos\gamma_3} + \frac{hz_3}{x_1\sin\gamma_2 + y_1\cos\gamma_2}, \tag{40a}$$

$$= \frac{hz_1}{x_2\sin\gamma_3 - y_2\cos\gamma_3} + \frac{hz_2}{y_2} + \frac{hz_3}{x_2\sin\gamma_1 + y_2\cos\gamma_1}. \tag{40b}$$

The intervals of variation (25) and the boundary conditions (26) remain unchanged.

Hyperspherical coordinates. Relations (28) and (29) take the form

$$\begin{aligned} x &= r\cos h\phi, \\ y &= r\sin h\phi, \end{aligned} \quad \leftrightarrow \quad \begin{aligned} r &= \sqrt{x^2+y^2}, \\ \phi &= h^{-1}\arctan(y/x), \end{aligned} \tag{41}$$

and

$$\phi_1 + \phi_2 = \pi/2. \tag{42}$$

The kinetic (30) and potential (31) energies become

$$T = -\frac{h^2}{2r}\frac{\partial}{\partial r}r\frac{\partial}{\partial r} - \frac{1}{2r^2}\frac{\partial^2}{\partial\phi^2} \tag{43}$$

and

$$V = \frac{1}{r}\left(\frac{hz_1}{\sin[h\phi_1]} + \frac{hz_2}{\sin[h(\pi/2-\phi_1)]} + \frac{hz_3}{\cos[h(\phi_1-\pi(1-\varepsilon)/4)]}\right), \tag{44a}$$

$$= \frac{1}{r}\left(\frac{hz_1}{\sin[h(\pi/2-\phi_2)]} + \frac{hz_2}{\sin[h\phi_2]} + \frac{hz_3}{\cos[h(\phi_2-\pi(1+\varepsilon)/4)]}\right). \tag{44b}$$

The intervals of variation (32) are changed to

$$0 \le r < \infty, \quad 0 \le \phi \le \pi/2, \tag{45}$$

and the boundary conditions (33) read

$$\Psi(r,\phi)|_{\phi=0} = \Psi(r,\phi)|_{\phi=\pi/2} = 0. \tag{46}$$

G. Permutation symmetry in the symmetric case

The symmetric case (case A when particles 1 and 2 are identical) requires a special consideration. In this case, Eq. (2) remains unchanged under the permutation of X_1 and X_2. As can bee seen from Eqs. (20), such permutation corresponds to $(x_1, y_1) \to (-x_2, -y_2)$ in Jacobi coordinates. However, if the initial point (x_1, y_1) lies inside the sector (25), its image $(-x_2, -y_2)$ falls outside it. We can return back to the sector (25) by the inversion $(X_1, X_2, X_3) \to (-X_1, -X_2, -X_3)$ which also leaves Eq. (2) unchanged. This corresponds to $(-x_2, -y_2) \to (x_2, y_2)$ in Jacobi coordinates. The composition of these two transformations, $(x_1, y_1) \to (x_2, y_2)$, amounts to mirror reflection of the sector (25) with respect to the line $y = x\tan(\gamma/2)$. The solutions of Eq. (13) can be chosen to be either even or odd under such reflection. Even (odd) solutions will be indicated by the subscript $\sigma = +(-)$. They satisfy

$$\Psi_\sigma(x_1, y_1) = \sigma\Psi_\sigma(x_2, y_2). \tag{47}$$

This relation can be presented in the form of boundary conditions on the line $y = x\tan(\gamma/2)$,

$$\begin{aligned} \left[\sin(\gamma/2)\frac{\partial}{\partial x} - \cos(\gamma/2)\frac{\partial}{\partial y}\right] \Psi_+(x,y)\Big|_{y=x\tan(\gamma/2)} &= 0, \\ \Psi_-(x,y)|_{y=x\tan(\gamma/2)} &= 0. \end{aligned} \tag{48}$$

In hyperspherical coordinates, these conditions read

$$\begin{aligned} \frac{\partial\Psi_+(r,\phi)}{\partial\phi}\Big|_{\phi=\pi/4} &= 0, \\ \Psi_-(r,\phi)|_{\phi=\pi/4} &= 0. \end{aligned} \tag{49}$$

Taking them into account, in the symmetric case it is sufficient to consider Eq. (13) only in a half of the sector (25), (45).

H. Asymptotic states

The disintegration of the system into two fragments in arrangement α occurs in the region $x_\alpha \to \infty$, $y_\alpha = \mathcal{O}(x_\alpha^0)$. Here, the potential energy (40) can be expanded in powers of x_α^{-1},

$$V = \frac{hz_\alpha}{y_\alpha} + \frac{hZ_\alpha}{x_\alpha} + \frac{hD_\alpha y_\alpha}{x_\alpha^2} + \mathcal{O}(x_\alpha^{-3}), \tag{50}$$

where Z_α are the asymptotic charges,

$$Z_1 = \frac{z_2}{\sin\gamma_3} + \frac{z_3}{\sin\gamma_2}, \tag{51a}$$

$$Z_2 = \frac{z_1}{\sin\gamma_3} + \frac{z_3}{\sin\gamma_1}, \tag{51b}$$

and D_α are the asymptotic dipole momenta,

$$D_1 = z_2\frac{\cos\gamma_3}{\sin^2\gamma_3} - z_3\frac{\cos\gamma_2}{\sin^2\gamma_2}, \tag{52a}$$

$$D_2 = z_1\frac{\cos\gamma_3}{\sin^2\gamma_3} - z_3\frac{\cos\gamma_1}{\sin^2\gamma_1}. \tag{52b}$$

Retaining only first two terms in Eq. (50) and substituting them into Eq. (13) we obtain

$$\left[-\frac{h^2}{2}\frac{\partial^2}{\partial x_\alpha^2} - \frac{h^2}{2}\frac{\partial^2}{\partial y_\alpha^2} + \frac{hz_\alpha}{y_\alpha} + \frac{hZ_\alpha}{x_\alpha} - E\right]\Psi(x_\alpha, y_\alpha) = 0. \tag{53}$$

Asymptotic states are the elementary solutions to this equation defining physical asymptotic boundary conditions for scattering processes. They can be found by separating variables x_α and y_α. In this work we consider only the solutions for $E < 0$. The regular (s) and irregular (c) at $x_\alpha = 0$ solutions are given by

$$\Psi^{(s,c)}_{\nu_{\rm as}}(x_\alpha, y_\alpha) = (h/k_{\alpha n})^{1/2}\mathcal{F}^{(s,c)}(k_{\alpha n}x_\alpha/h; Z_\alpha/k_{\alpha n}) \times (|z_\alpha|/h)^{1/2}\,\mathcal{B}_n(|z_\alpha|y_\alpha/h), \tag{54}$$

$$\nu_{\rm as} = (\alpha, n), \qquad \alpha = 1, 2, \qquad n = 1, 2, \ldots.$$

The two factors here describe the relative motion of the free particle and the bound pair and the internal state of the bound pair, respectively, where $\nu_{\rm as}$ identifies asymptotic channels, with α and n specifying arrangement and state of the bound pair, $k_{\alpha n}$ is the channel momentum,

$$k_{\alpha n}^2 = 2(E - v_{\alpha n}), \tag{55}$$

$v_{\alpha n}$ is the channel threshold energy,

$$v_{\alpha n} = -\frac{{z_\alpha}^2}{2n^2}, \tag{56}$$

and functions $\mathcal{B}_n(x)$ and $\mathcal{F}^{(s,c)}(x;\eta)$ are defined in appendices A1a and A2a, respectively. Functions (54) satisfy the first of conditions (26), but they do not satisfy the second one. However, the second condition is satisfied asymptotically for $x_\alpha \to \infty$, because $\mathcal{B}_n(x)$ exponentially decays for large values of its argument. In the symmetric case, in order to satisfy Eq. (47) we introduce symmetrized asymptotic states,

$$\Psi^{(s,c)}_{\sigma n}(\mathbf{r}) = \frac{1}{\sqrt{2}}\left(\Psi^{(s,c)}_{1n}(x_1,y_1) + \sigma\Psi^{(s,c)}_{2n}(x_2,y_2)\right). \tag{57}$$

Now we can complete the definition of cases A, B1, and B2. The following table summarizes our conventions in terms of pair charges z_i:

$$\begin{array}{lll} \text{case A:} & z_1 \le z_2 < 0, & 0 < z_3, \\ \text{case B1:} & 0 < z_2, & z_1 \le z_3 < 0, \\ \text{case B2:} & 0 < z_2, & z_3 \le z_1 < 0. \end{array} \tag{58}$$

The physical meaning of these conditions can be seen from Eq. (56). In case A, we assume that the hydrogenic spectrum of the bound pair in arrangement 1 lies lower or coincides with that in arrangement 2, which is always possible to achieve by interchanging particles 1 and 2, and cases B1 and B2 are distinguished by the relative position of the hydrogenic spectra in pairs 1 and 3 (note that with the assumed order of particles pair 3 cannot be separated from the remaining particle 3). Thus in all the cases the lowest channel is $(\alpha, n) = (1, 1)$. Taking into account that $z_1 = -1$, see Eqs. (38), from Eq. (56) we have $v_{11} = -0.5$, which defines the threshold energy for disintegration into two fragments.

I. Asymptotic boundary conditions

We are interested in the solutions of Eq. (13) which apart from the regularity boundary conditions (26), (46) satisfy appropriate physical boundary conditions in the asymptotic region $r \to \infty$. Let us formulate these conditions.

For bound states, the wave function must vanish at large separations between any two particles, therefore

$$\Psi(\mathbf{r})|_{r\to\infty} = 0. \tag{59}$$

The solutions of Eq. (13) satisfying conditions (26), (46), and (59) simultaneously may exist only for discrete values of E, hence we obtain an eigenvalue problem (EVP). The purpose of program CTBC in the bound case is to calculate bound state eigenvalues and eigenfunctions.

For scattering states in the energy range $-0.5 < E < 0$, the physical asymptotic boundary conditions are formulated in terms of the asymptotic states (54),

$$\Psi_{\nu_{as}}(\mathbf{r})|_{r\to\infty} = \Psi^{(s)}_{\nu_{as}}(\mathbf{r}) + \sum_{\mu_{as}}^{\text{open}} \Psi^{(c)}_{\mu_{as}}(\mathbf{r}) K_{\mu_{as}\nu_{as}}, \tag{60}$$

where summation goes over all open channels (a channel is open if $E > v_{\alpha n}$, otherwise it is closed). Equation (60) defines the reactance matrix $\mathbf{K}$ which is related to the scattering matrix $\mathbf{S}$ by [1]

$$\mathbf{S} = \frac{1 + i\mathbf{K}}{1 - i\mathbf{K}}. \tag{61}$$

In case A, matrix $\mathbf{S}$ can be partitioned into four blocks according to the index α specifying arrangements,

$$\mathbf{S} = \begin{pmatrix} \mathbf{S}^{(11)} & \mathbf{S}^{(12)} \\ \mathbf{S}^{(21)} & \mathbf{S}^{(22)} \end{pmatrix}. \tag{62}$$

In case B, there is only one arrangement $\alpha = 1$, therefore only one block $\mathbf{S}^{(11)}$ is present. In the symmetric case, the boundary conditions (60) can be reformulated in terms of the symmetrized asymptotic states (57),

$$\Psi_{\sigma n}(\mathbf{r})|_{r\to\infty} = \Psi^{(s)}_{\sigma n}(\mathbf{r}) + \sum_{m}^{\text{open}} \Psi^{(c)}_{\sigma m}(\mathbf{r}) K^{(\sigma)}_{mn}. \tag{63}$$

Note that there are no transitions between states with different permutation symmetry. Equation (63) defines the reactance matrix $\mathbf{K}^{(\sigma)}$, and the corresponding scattering matrix $\mathbf{S}^{(\sigma)}$ is again given by Eq. (61). In this case, matrix $\mathbf{S}$ can be partitioned into blocks according to the permutation symmetry index σ,

$$\mathbf{S} = \begin{pmatrix} \mathbf{S}^{(+)} & \mathbf{0} \\ \mathbf{0} & \mathbf{S}^{(-)} \end{pmatrix}. \tag{64}$$

As follows from Eq. (57), representations (62) and (64) are related by

$$\mathbf{S}^{(11)} = \mathbf{S}^{(22)} = \tfrac{1}{2}\left(\mathbf{S}^{(+)} + \mathbf{S}^{(-)}\right), \tag{65a}$$

$$\mathbf{S}^{(12)} = \mathbf{S}^{(21)} = \tfrac{1}{2}\left(\mathbf{S}^{(+)} - \mathbf{S}^{(-)}\right). \tag{65b}$$

The purpose of program CTBC in the scattering case is to calculate scattering matrix $\mathbf{S}$.

III. HYPERSPHERICAL ADIABATIC (HSA) APPROACH

This approach [2] to the solution of the Schrödinger equation for a few-body system is based on the adiabatic expansion of the wave function in hyperspherical coordinates, with hyperradius and hyperangles treated as "slow" and "fast" variables, respectively. It suggests a consistent computational scheme which enables one, at least in principle, to obtain accurate solutions of Eq. (13) for $E < 0$. The SVD method used to solve Eq. (13) in CTBC, see next section, is intimately related to the HSA approach, so before describing the former it is useful to recall main steps of the latter. To this end, let us rewrite Eqs. (13), (43), and (44) in the form

$$\left[-\frac{h^2}{2r}\frac{\partial}{\partial r}r\frac{\partial}{\partial r}+\frac{\mathcal{U}(r)}{r^2}-E\right]\Psi(r,\phi)=0, \tag{66}$$

where $\mathcal{U}(r)$ is the HSA Hamiltonian,

$$\mathcal{U}(r)=-\frac{1}{2}\frac{\partial^2}{\partial\phi^2}+rC(\phi), \tag{67}$$

and $C(\phi)$ is the effective charge,

$$C(\phi) = \frac{hz_1}{\sin[h\phi_1]}+\frac{hz_2}{\sin[h(\pi/2-\phi_1)]}+\frac{hz_3}{\cos[h(\phi_1-\pi(1-\varepsilon)/4)]}, \tag{68a}$$

$$= \frac{hz_1}{\sin[h(\pi/2-\phi_2)]}+\frac{hz_2}{\sin[h\phi_2]}+\frac{hz_3}{\cos[h(\phi_2-\pi(1+\varepsilon)/4)]}. \tag{68b}$$

The notation $\mathcal{U}(r)$ emphasizes that this operator parametrically depends on r. Note that for any fixed value of ε we have

$$C(\phi)|_{h\to 0}=-\frac{1}{\phi_1}-\frac{e_1}{e_2\phi_2}-\frac{2e_1}{\pi e_3}+\mathcal{O}(h^2). \tag{69}$$

Thus in the limit $h\to 0$ the parameter h enters into Eq. (66) only in the form of an effective Planck's constant for the motion in r, which renders Eq. (66) amenable to the analysis by asymptotic methods. This circumstance justifies scaling (36).

A. HSA eigenvalue problem

First in the HSA approach is treated the motion in angular variable ϕ for a fixed value of hyperradius r. This motion is described by the HSA EVP

$$[\mathcal{U}(r)-U(r)]\,\Phi(\phi;r)=0, \tag{70a}$$

$$\Phi(0;r)=\Phi(\pi/2;r)=0, \tag{70b}$$

where, again, the argument r shows that the eigenvalue $U(r)$ and eigenfunction $\Phi(\phi;r)$ depend on r as a parameter. The solutions to Eq. (70) will be denoted by

$$U_\nu(r), \quad \Phi_\nu(\phi;r), \qquad \nu = 1,2,\ldots \tag{71}$$

For any r, the eigenfunctions form a complete set in the space of square integrable functions in the interval $0 \le \phi \le \pi/2$. We normalize them by

$$\langle \Phi_\nu(\phi;r)|\Phi_\mu(\phi;r)\rangle = \delta_{\nu\mu}, \tag{72}$$

where

$$\langle \ldots \rangle \equiv \frac{4}{\pi}\int_0^{\pi/2} \ldots d\phi. \tag{73}$$

In two limiting cases the solutions can be found analytically. For $r \to 0$ we have

$$\begin{aligned} &U_\nu(r)|_{r\to 0} = 2\nu^2 + rC_\nu + \mathcal{O}(r^2), \\ &\Phi_\nu(\phi;r)|_{r\to 0} = \sin(2\nu\phi), \end{aligned} \tag{74}$$

where $C_\nu = C_{\nu\nu}(0)$ and

$$C_{\nu\mu}(r) = \langle \Phi_\nu(\phi;r)|C(\phi)|\Phi_\mu(\phi;r)\rangle = C_{\mu\nu}(r). \tag{75}$$

For $r \to \infty$, using the expansion

$$C(\phi_\alpha)|_{\phi_\alpha\to 0} = \frac{z_\alpha}{\phi_\alpha} + hZ_\alpha + h^2\left(D_\alpha + z_\alpha/6\right)\phi_\alpha + \mathcal{O}({\phi_\alpha}^2), \tag{76}$$

we obtain

$$\begin{aligned} &U_{\nu_{\rm as}}(r)|_{r\to\infty} = -\frac{z_\alpha^2 r^2}{2n^2} + hZ_\alpha r + h^2 n^2\left(\frac{3D_\alpha}{2|z_\alpha|} - \frac{1}{4}\right) + \mathcal{O}(r^{-1}), \\ &\Phi_{\nu_{\rm as}}(\phi_\alpha;r)|_{r\to\infty} = \tfrac{1}{2}(\pi|z_\alpha|r)^{1/2}\mathcal{B}_n(|z_\alpha|r\phi_\alpha), \\ &\nu_{\rm as} = (\alpha,n), \qquad \alpha = 1,2, \quad n = 1,2,\ldots, \end{aligned} \tag{77}$$

where the function $\mathcal{B}_n(x)$ is defined in appendix A1a.

B. HSA expansion

Second in the HSA approach is treated the motion in hyperradius r. Let us rewrite Eq. (66) as

$$\left[-\frac{h^2}{2}\frac{\partial^2}{\partial r^2} + \frac{\mathcal{U}(r) - h^2/8}{r^2} - E\right] r^{1/2}\Psi(r,\phi) = 0. \tag{78}$$

The solutions to this equation are sought in the form of the HSA expansion

$$\Psi(r,\phi) = r^{-1/2} \sum_{\nu} F_{\nu}(r) \Phi_{\nu}(\phi;r). \tag{79}$$

Substituting this into Eq. (78), one obtains a set of ordinary differential equations defining the functions $F_{\nu}(r)$,

$$\left[-\frac{h^2}{2} \frac{d^2}{dr^2} + V_{\nu}(r) - E \right] F_{\nu}(r) = \frac{h^2}{2} \sum_{\mu} \left[2P_{\nu\mu}(r) \frac{d}{dr} + Q_{\nu\mu}(r) \right] F_{\mu}(r), \tag{80}$$

where

$$V_{\nu}(r) = \frac{U_{\nu}(r) - h^2/8}{r^2} \tag{81}$$

are the HSA potentials and

$$P_{\nu\mu}(r) = \left\langle \Phi_{\nu}(\phi;r) \middle| \frac{\partial \Phi_{\mu}(\phi;r)}{\partial r} \right\rangle = -P_{\mu\nu}(r), \quad P_{\nu\nu}(r) = 0, \tag{82}$$

$$Q_{\nu\mu}(r) = \left\langle \Phi_{\nu}(\phi;r) \middle| \frac{\partial^2 \Phi_{\mu}(\phi;r)}{\partial r^2} \right\rangle, \tag{83}$$

are the matrices of nonadiabatic couplings. Introducing an additional matrix,

$$Q^{(s)}_{\nu\mu}(r) = \left\langle \frac{\partial \Phi_{\nu}(\phi;r)}{\partial r} \middle| \frac{\partial \Phi_{\mu}(\phi;r)}{\partial r} \right\rangle = Q^{(s)}_{\mu\nu}(r), \tag{84}$$

we obtain the relations

$$Q^{(s)}_{\nu\mu}(r) = \sum_{\lambda} P_{\lambda\nu}(r) P_{\lambda\mu}(r), \tag{85}$$

$$Q_{\nu\mu}(r) + Q^{(s)}_{\nu\mu}(r) = \frac{P_{\nu\mu}(r)}{dr}. \tag{86}$$

Using the perturbation theory, it can be shown that

$$P_{\nu\mu}(r) = \frac{-C_{\nu\mu}(r)}{U_{\nu}(r) - U_{\mu}(r)}, \qquad \nu \neq \mu. \tag{87}$$

Solving Eqs. (80) with appropriate boundary conditions and substituting the solution into (79), one obtains a solution to Eq. (78). In practical calculations, only a finite number of HSA channels $N_{\rm ch}$ can be retained in expansion (79) . However, completeness of the HSA basis (71) ensures that this expansion converges as $N_{\rm ch}$ grows. The main advantage of the HSA approach stems from the observation that in many situations expansion (79) converges more rapidly than it could be a priori expected. Its difficulties are hidden in the solution of equations (80).

IV. SLOW/SMOOTH VARIABLE DISCRETIZATION (SVD) METHOD

This method [3] of solving the Schrödinger equation applies to systems whose Hamiltonians allow adiabatic separation of variables. It is based on the expansion of the wave function in a concerted combination of the adiabatic basis for "fast" variables and a DVR basis for the "slow" one. In application to the present problem, SVD preserves all advantages of the HSA approach leaving aside its difficulties. Let us introduce a new function

$$\psi(r,\phi) = r^{-1/2}\Psi(r,\phi) \tag{88}$$

and rewrite Eq. (66) as

$$\left[-\frac{h^2}{2}\frac{\partial}{\partial r}r^2\frac{\partial}{\partial r} + \mathcal{U}(r) - \frac{h^2}{8} - Er^2\right]\psi(r,\phi) = 0. \tag{89}$$

Suppose we wish to find a general solution to this equation in the interval

$$r_a \le r \le r_b. \tag{90}$$

As a first step, r must be replaced by a new variable t,

$$r = r(t) \quad \leftrightarrow \quad t = t(r). \tag{91}$$

The purpose of this transformation is to map the interval (90) into the interval of orthogonality $a \le t \le b$ for a suitable set of COP, see appendix B1. Only linear transformations will be used here; let us introduce notation

$$dr(t)/dt = s. \tag{92}$$

Then the type of COP is uniquely defined by the interval (90) and the boundary conditions for the wave function $\psi(r,\phi)$ at its ends. Let t_i and $\pi_i(t)$, $i = 1,\ldots,N_r$, be the corresponding N_r-point Gaussian quadrature and DVR basis, and $r_i = r(t_i)$. Note that this basis becomes complete in the space of square integrable functions in the interval (90) as $N_r \to \infty$.

A. SVD eigenvalue problem

Let us introduce a Bloch operator [4],

$$\mathcal{L} = \frac{h^2}{2}r^2\left[\delta(r-r_b) - \delta(r-r_a)\right]\frac{\partial}{\partial r}, \tag{93}$$

and consider the equation

$$\left[-\frac{h^2}{2}\frac{\partial}{\partial r}r^2\frac{\partial}{\partial r}+\mathcal{L}+\mathcal{U}(r)-\frac{h^2}{8}-\bar{E}r^2\right]\bar{\psi}(r,\phi)=0, \tag{94}$$

which differs from Eq. (89) by the term with $\mathcal{L}$. The solutions to this equation are sought in the form of the SVD expansion

$$\bar{\psi}(r,\phi)=\sum_{i\nu}c_{i\nu}\pi_i(t)\Phi_\nu(\phi;r_i), \tag{95}$$

where $\Phi_\nu(\phi;r)$ are HSA basis functions defined by Eq. (70). Substituting this into Eq. (94) and using (B16) and (B19), one obtains an algebraic SVD EVP defining the coefficients $c_{i\nu}$,

$$\sum_{j\mu}\left(h^2K_{ij}-\bar{E}s^2\rho_{ij}\right)O_{i\nu,j\mu}c_{j\mu}+[U_\nu(r_i)-h^2/8]c_{i\nu}=0, \tag{96}$$

where K_{ij} and ρ_{ij} are the DVR kinetic and weight matrices,

$$K_{ij} = \frac{1}{2s^2}\int_a^b\frac{d\pi_i(t)}{dt}\,r^2(t)\,\frac{d\pi_j(t)}{dt}\,dt, \tag{97}$$

$$\rho_{ij} = \frac{1}{s^2}\int_a^b\pi_i(t)r^2(t)\pi_j(t)\,dt, \tag{98}$$

and $O_{i\nu,j\mu}$ is the overlap matrix for HSA bases at different quadrature points,

$$O_{i\nu,j\mu}=\langle\Phi_\nu(\phi;r_i)|\Phi_\mu(\phi;r_j)\rangle. \tag{99}$$

Let $c^n_{i\nu}$ be the eigenvectors of Eq. (96); we normalize them by

$$s^3\sum_{i\nu}\sum_{j\mu}c^n_{i\nu}c^m_{j\mu}\rho_{ij}O_{i\nu,j\mu}=\delta_{nm}. \tag{100}$$

The corresponding solutions to Eq. (94) will be denoted by

$$\bar{E}_n,\quad \bar{\psi}_n(r,\phi),\qquad n=1,2,\ldots \tag{101}$$

The eigenfunctions satisfy

$$\langle\langle\bar{\psi}_n(r,\phi)|r^2|\bar{\psi}_m(r,\phi)\rangle\rangle=\delta_{nm}, \tag{102}$$

where

$$\langle\langle\ldots\rangle\rangle\equiv\int_{r_a}^{r_b}\langle\ldots\rangle\,dr. \tag{103}$$

Similar to Eq. (79), they can be expanded in HSA basis,

$$\bar{\psi}_n(r,\phi)=r^{-1}\sum_\nu\bar{F}_{\nu n}(r)\Phi_\nu(\phi;r). \tag{104}$$

Comparing this with Eq. (95) and taking into account property (B15), we obtain a relation between $\bar{F}_{\nu n}(r)$ and $c^n_{i\nu}$,

$$\bar{F}_{\nu n}(r_i)=r_i\kappa_i^{-1}c^n_{i\nu}. \tag{105}$$

B. SVD solution

In the SVD method, the solutions of Eq. (89) in the interval (90) are sought in the form of expansion in terms of $\bar{\psi}_n(r,\phi)$. It can be shown that an arbitrary solution satisfies

$$\psi(r,\phi) = \sum_n \frac{\langle\langle \bar{\psi}_n(r,\phi)|\mathcal{L}|\psi(r,\phi)\rangle\rangle}{\bar{E}_n - E}\bar{\psi}_n(r,\phi). \tag{106}$$

From this, for a particular solution defined by the boundary conditions

$$\left\langle \Phi_\nu(\phi;r)\left|\frac{\partial\psi(r,\phi)}{\partial r}\right\rangle\right|_{r=r_{a,b}} = d_\nu^{a,b}, \qquad \nu = 1,2,\ldots, \tag{107}$$

we obtain

$$\psi(r,\phi) = \frac{h^2}{2}\sum_n \frac{\bar{\psi}_n(r,\phi)}{\bar{E}_n - E}\sum_\nu \left[r_b\bar{F}_{\nu n}(r_b)d_\nu^b - r_a\bar{F}_{\nu n}(r_a)d_\nu^a\right], \tag{108}$$

where

$$\bar{F}_{\nu n}(r_{a,b}) = r_{a,b}\sum_{j\mu} c_{j\mu}^n \pi_j(a,b) O_{\nu,j\mu}^{a,b}, \tag{109}$$

and

$$O_{\nu,j\mu}^{a,b} = \langle\Phi_\nu(\phi;r_{a,b})|\Phi_\mu(\phi;r_j)\rangle. \tag{110}$$

In these formulas 'a,b' stands for one of a or b. Treating d_ν^a and d_ν^b as arbitrary constants, Eq. (108) gives a general solution of Eq. (89) in the interval (90). There are two cases that require a special consideration. First, if energy E in Eq. (89) coincides with one of the eigenvalues $\bar{E}_n$ of Eq. (94), the coefficient in the corresponding term in (106) is arbitrary, and the solution is not defined uniquely. Second, if d_ν^a and d_ν^b are such that all the coefficients in (106) are zero, we obtain an eigenvalue problem: a solution to Eqs. (89) and (107) in this case exists only if E coincides with one of $\bar{E}_n$ and is given by $\bar{\psi}_n(r,\phi)$.

In practical calculations, expansion (95) contains a finite number $N_{\rm SVD} = N_r \times N_{\rm ch}$ of terms, where N_r is the dimension of the DVR basis and $N_{\rm ch}$ is the number of HSA channels. Thus solving Eq. (96) one obtains $N_{\rm SVD}$ SVD solutions (101). Due to completeness of the DVR and HSA bases, these solutions form a complete set in the space of functions square integrable in the region $r_a \le r \le r_b$, $0 \le \phi \le \pi/2$ as both N_r and $N_{\rm ch}$ tend to infinity, which ensures convergence of expansion (108). The rate of this convergence with respect to N_r is as high as in the DVR method and that with respect to $N_{\rm ch}$ is the same as in the HSA approach.

V. NUMERICAL PROCEDURE

Here we discuss major elements of the numerical procedure used in CTBC, describe structure of the program, and specify recommended values of the input parameters.

A. Solution of HSA eigenvalue problem

The HSA EVP (70) explicitly reads

$$\left[-\frac{1}{2}\frac{\partial^2}{\partial\phi^2} + rC(\phi) - U(r)\right]\Phi(\phi;r) = 0, \tag{111a}$$

$$\Phi(0;r) = \Phi(\pi/2;r) = 0. \tag{111b}$$

Let us introduce a new variable,

$$\begin{array}{c} \phi(t) = \pi(1+t)/4, \\ 0 \le \phi \le \pi/2, \end{array} \quad \leftrightarrow \quad \begin{array}{c} t(\phi) = 4\phi/\pi - 1, \\ -1 \le t \le 1, \end{array} \tag{112}$$

and rewrite Eq. (111) in the standard form (B23),

$$\left[\frac{d}{dt}(1-t^2)\frac{d}{dt} - \frac{1}{1-t^2} + \frac{\pi^2}{8}(1-t^2)\left(U(r) - rC(\phi)\right)\right]\frac{\Phi(\phi;r)}{\sqrt{1-t^2}} = 0. \tag{113}$$

We solve this equation by the DVR method using N_ϕ-point Jacobi $P_n^{(\alpha,\beta)}(t)$ quadrature. The parameters of the Jacobi polynomials are uniquely determined by the condition that $\Phi(\phi;r)$ must linearly vanish at the ends of the interval (112), which yields $\alpha = \beta = 1$. The polynomials of even/odd order are even/odd functions of t, so the permutation symmetry boundary conditions (49) in the symmetric case can be easily implemented. The solutions are obtained in the form

$$U_\nu(r), \quad \Phi_\nu(\phi;r) = \sqrt{1-t^2}\sum_{i=1}^{N_\phi}\frac{c_i^\nu(r)}{\sqrt{1-t_i^2}}\pi_i(t), \qquad \nu = 1,2,\ldots,N_\phi. \tag{114}$$

The eigenvectors $c_i^\nu(r)$ are normalized by

$$\sum_{i=1}^{N_\phi} c_i^\nu(r)c_i^\mu(r) = \delta_{\nu\mu}. \tag{115}$$

Then

$$\langle\Phi_\nu(\phi;r)|\Phi_\mu(\phi;r)\rangle \approx \delta_{\nu\mu}, \tag{116}$$

in accord with Eq. (72), where the approximation amounts to the use of quadrature (B7). With the same accuracy, the overlap matrices (99) and (110) can be calculated using

$$\langle \Phi_\nu(\phi;r)|\Phi_\mu(\phi;r')\rangle \approx \sum_{i=1}^{N_\phi} c_i^\nu(r) c_i^\mu(r'), \tag{117}$$

and the potential energy matrix (75) is given by

$$C_{\nu\mu}(r) \approx \sum_{i=1}^{N_\phi} c_i^\nu(r) C(\phi_i) c_i^\mu(r), \tag{118}$$

where $\phi_i = \phi(t_i)$. Taking into account property (B15), at the quadrature points we have

$$\Phi_\nu(\phi_i;r) = \kappa_i^{-1} c_i^\nu(r). \tag{119}$$

We solve Eq. (111) using angular variable ϕ_1 from the 1st Jacobi set. The main limitation of the procedure described above stems from the fact that for large values of r functions $\Phi_\nu(\phi_1;r)$ are localized in small intervals of ϕ_1 near $\phi_1 = 0$ (arrangement $\alpha = 1$) or $\phi_1 = \pi/2$ (arrangement $\alpha = 2$) whose size is $\propto 1/r$, see Eqs. (77). This situation is similar to that discussed in appendix A1b. To cope with the localization problem the dimension of the DVR basis must grow $\propto \sqrt{r}$,

$$N_\phi = \eta\sqrt{r}, \tag{120}$$

where the coefficient η depends on the accuracy required. We have found the following dependence between η and the relative accuracy of the lowest eigenvalue $U_1(r)$,

$$\eta = 4.0 \;\rightarrow\; \delta U_1/U_1 < 10^{-6}, \tag{121a}$$

$$\eta = 4.5 \;\rightarrow\; \delta U_1/U_1 < 10^{-8}. \tag{121b}$$

This agrees with Eqs. (A20) and (A21), where one must substitute $a = r\pi/2$.

B. Bound state calculations

In the calculation of bound states, Eq. (89) is considered in the interval $0 \le r < \infty$. The transformation (91) in this case is defined by

$$\begin{array}{l} r(t) = st, \\ 0 \le r < \infty, \end{array} \quad \leftrightarrow \quad \begin{array}{l} t(r) = r/s, \\ 0 \le t < \infty, \end{array} \tag{122}$$

where

$$s = r_{\rm m}/t_{N_r}. \tag{123}$$

Here t_{N_r} is the last quadrature point for the given dimension N_r of the DVR basis, and the parameter $r_{\rm m}$ characterizes the size of the region where bound state wave functions to be found are localized. A suitable DVR basis can be constructed from Laguerre polynomials $L_n^{(\alpha)}(t)$. Then function (95) exponentially decays as $r \to \infty$, which is in accord with Eq. (59), and behaves $\propto r^{\alpha/2}$ as $r \to 0$. Taking into account Eq. (88), in order to satisfy Eq. (35) we would have to put $\alpha = 2\pi/\gamma - 1$, which gives growing values of α for $\gamma \to 0$. However, the interval of r where the power behavior (35) holds decreases as $\gamma \to 0$, and large values of the exponent in this case indicate that the wave function decays actually exponentially under the centrifugal barrier, hence there is no point to strictly observe Eq. (35) in numerical calculations. In CTBC we use $\alpha = 3$ which corresponds to the largest possible $\gamma = \pi/2$. In thus defined DVR basis, matrices (97) and (98) can be calculated analytically, see appendix B3. Bound states are represented by the solutions of Eq. (96) with eigenvalues $\bar{E}_n < -0.5$. Convergence of the eigenvalues with respect to the dimension of radial DVR basis N_r is as fast as in applications of DVR to the calculation of bound states in a simple one-channel potential well; it is sufficient to have 6-8 quadrature points per half of the wave length for the highest bound state desired. Convergence with respect to the number of HSA channels $N_{\rm ch}$ depends on the system; the value of $N_{\rm ch}$ required varies from several units (~ 3) to several tens (~ 30) for systems with $h \ll 1$ and $h \sim 1$, respectively. A typical value of $r_{\rm m}$ for the ground state is 50-100.

C. Scattering calculations

For energies below the three-body disintegration threshold, the solutions of Eq. (13) exponentially decay as $r \to \infty$ except for near two singular directions at $\phi = 0$ and $\phi = \pi/2$, where asymptotic states (54) representing disintegration of the system into two fragments are localized. In order to reproduce this asymptotic behaviour in the numerical solution, we divide configuration space into parts as shown in Fig. 3 and following [5] assume that the wave function vanishes in the hatched area. In the calculation of scattering, Eq. (13) is solved separately in the internal region and in asymptotic regions corresponding to each of the arrangements. The internal and asymptotic solutions are then matched along the

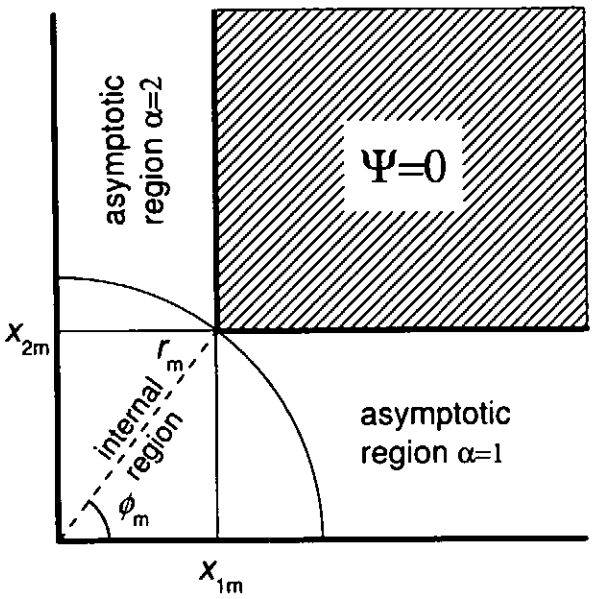

FIG. 3: The division of configuration space into parts used in scattering calculations. The wave function is assumed to vanish in the hatched area.

arc $r = r_{\rm m}$, where they are valid simultaneously, to construct a global solution satisfying Eq. (60), from which the scattering matrix is obtained.

1. Internal region

In the internal region hyperspherical coordinates are used, see Fig. 3. This region is defined by

$$0 \le r \le r_{\rm m}, \qquad 0 \le \phi \le \pi/2, \tag{124}$$

where $r_{\rm m}$ is the matching radius. This interval of r is divided into $N_{\rm sec}$ sectors with boundaries at $\bar{r}_k$,

$$0 = \bar{r}_0 < \bar{r}_1 < \bar{r}_2 < \ldots < \bar{r}_{N_{\rm sec}} = r_{\rm m}. \tag{125}$$

Within each sector, the solutions of Eq. (89) are found by the SVD method. The information obtained is then used to calculate the $\mathcal{R}$-matrix at the matching arc $r = r_{\rm m}$.

SVD EVP in a sector. Consider the k-th sector, $\bar{r}_{k-1} \le r \le \bar{r}_k$. Here, the transformation (91) is defined by

$$\begin{array}{l} r(t) = s(t_c + t), \\ \bar{r}_{k-1} \le r \le \bar{r}_k, \end{array} \quad \leftrightarrow \quad \begin{array}{l} t(r) = r/s - t_c, \\ -1 \le t \le 1, \end{array} \tag{126}$$

where

$$s = \tfrac{1}{2}(\bar{r}_k - \bar{r}_{k-1}), \qquad t_c = \frac{\bar{r}_k + \bar{r}_{k-1}}{\bar{r}_k - \bar{r}_{k-1}}. \tag{127}$$

In the first sector, a suitable DVR basis can be constructed from Jacobi polynomials $P_n^{(\alpha,\beta)}(t)$. For the same reasons as in the case of bound states we put $\beta = 3$, which is in accord with Eq. (35) for $\gamma = \pi/2$. In order to satisfy arbitrary boundary conditions at the right end of this sector we put $\alpha = 0$. In all further sectors, radial DVR basis is constructed from Legendre polynomials $P_n(t) = P_n^{(0,0)}(t)$. Matrices (97) and (98) in this case also can be calculated analytically, see appendix B3. Solving Eq. (96), we obtain $N_{\rm SVD}$ solutions (101) from which the SVD surface amplitudes $\bar{F}_{\nu n}(\bar{r}_k)$ and $\bar{F}_{\nu n}(\bar{r}_{k-1})$ are calculated using Eq. (109). There is certain dependence between the dimension of radial DVR basis N_r and sector size: increasing the latter one must simultaneously increase the former. On the other hand, choosing sector size one must take into account that the wave length of radial oscillations of the wave function is proportional to h. We recommend the following combination of these parameters: sector size $h\pi$, which is equal to half of the wave length in the asymptotic region in the 1st channel for $E = 0$, and then $N_r =$ 6-8, similar to the bound case.

$\mathcal{R}$-matrix propagation. The $\mathcal{R}$-matrix [6] is defined by

$$\langle \Phi_\nu(\phi;r)|\psi(r,\phi)\rangle = \sum_\mu \mathcal{R}_{\nu\mu}(r)\left\langle \Phi_\mu(\phi;r)\left|\frac{\partial\psi(r,\phi)}{\partial r}\right.\right\rangle. \tag{128}$$

As follows from Eqs. (35) and (88),

$$\mathcal{R}(0) = 0, \tag{129}$$

which provides the initial condition for the $\mathcal{R}$-matrix propagation [7]. The propagation of $\mathcal{R}(r)$ through the k-th sector, i.e., from $r = \bar{r}_{k-1}$ to $r = \bar{r}_k$, is accomplished using

$$\mathcal{R}(\bar{r}_k) = \mathcal{R}^{kk} - \mathcal{R}^{k\,k-1}\left[\mathcal{R}^{k-1\,k-1} + \mathcal{R}(\bar{r}_{k-1})\right]^{-1}\mathcal{R}^{k-1\,k}, \tag{130}$$

where

$$\mathcal{R}^{kl}_{\nu\mu} = \frac{h^2}{2}\sum_{n=1}^{N_{\rm SVD}} \frac{\bar{F}_{\nu n}(\bar{r}_k)\bar{F}_{\mu n}(\bar{r}_l)}{\bar{E}_n - E}. \tag{131}$$

Repeating this procedure $N_{\rm sec}$ times, we obtain $\mathcal{R} \equiv \mathcal{R}(r_{\rm m})$, which is the final result of the computational procedure in the internal region.

2. Asymptotic regions

In the asymptotic regions Jacobi coordinates are used, see Fig. 3. These regions are defined by

$$x_{\alpha m} \le x_\alpha < +\infty, \quad 0 \le y_\alpha \le y_{\alpha m}, \tag{132}$$

where

$$x_{\alpha m} = r_m \cos(h\phi_{\alpha m}), \quad y_{\alpha m} = r_m \sin(h\phi_{\alpha m}), \tag{133}$$

and

$$\phi_{1m} = \phi_m, \quad \phi_{2m} = \pi/2 - \phi_m. \tag{134}$$

There is certain freedom in choosing the parameter ϕ_m; we define it by

$$\begin{aligned} &\text{case A:} \quad \left.\frac{dC(\phi_1)}{d\phi_1}\right|_{\phi_1=\phi_m} = 0, \\ &\text{case B:} \quad C(\phi_1)|_{\phi_1=\phi_m} = 0. \end{aligned} \tag{135}$$

In each of the asymptotic regions, the potential energy (40) can be expanded in a series,

$$V = \frac{hz_\alpha}{y_\alpha} + \frac{hZ_\alpha}{x_\alpha} + h\sum_{\lambda=1}^{\infty} V_\alpha^{(\lambda)} \frac{y_\alpha^\lambda}{x_\alpha^{\lambda+1}}, \tag{136}$$

where Z_α are the asymptotic charges (51) and

$$V_1^{(\lambda)} = \frac{z_2}{\sin\gamma_3}(\cot\gamma_3)^\lambda + \frac{z_3}{\sin\gamma_2}(-\cot\gamma_2)^\lambda, \tag{137a}$$

$$V_2^{(\lambda)} = \frac{z_1}{\sin\gamma_3}(\cot\gamma_3)^\lambda + \frac{z_3}{\sin\gamma_1}(-\cot\gamma_1)^\lambda. \tag{137b}$$

The asymptotic dipole momenta (52) are related to these coefficients by $D_\alpha = V_\alpha^{(1)}$. Retaining only Λ_α terms in this expansion, the Schrödinger equation (13) takes the form

$$\left[-\frac{h^2}{2}\frac{\partial^2}{\partial {x_\alpha}^2} - \frac{h^2}{2}\frac{\partial^2}{\partial {y_\alpha}^2} + \frac{hz_\alpha}{y_\alpha} + \frac{hZ_\alpha}{x_\alpha} - E\right]\Psi(x_\alpha, y_\alpha) = -h\sum_{\lambda=1}^{\Lambda_\alpha} V_\alpha^{(\lambda)} \frac{y_\alpha^\lambda}{x_\alpha^{\lambda+1}}\Psi(x_\alpha, y_\alpha). \tag{138}$$

The asymptotic states used in CTBC are approximate solutions to this equation given by

$$\tilde{\Psi}_{\nu_{as}}^{(s,c)}(x_\alpha, y_\alpha) = \sum_{m=1}^{N_\alpha} \mathcal{F}_m^{n(s,c)}\left(x_\alpha/h; N_\alpha, Z_\alpha, k_\alpha^2, \Lambda_\alpha, A_\alpha\right) \times |z_\alpha|^{1/2} \mathcal{B}_m(|z_\alpha| y_\alpha/h; a_\alpha), \tag{139}$$

$$\nu_{as} = (\alpha, n), \qquad \alpha = 1, 2, \qquad n = 1, 2, \ldots, N_\alpha,$$

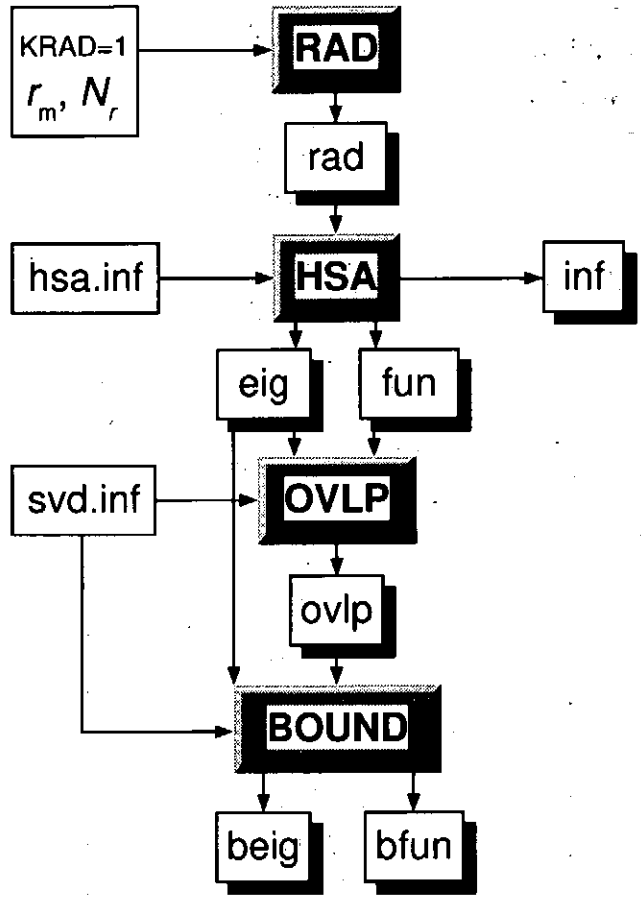

FIG. 4: CTBC executing sequence for bound state calculations.

where functions $\mathcal{B}_n(x;a)$ and $\mathcal{F}_m^{n(s,c)}(x;N,Z,k^2,\Lambda,A)$ are defined in appendices A1b and A2b, and the parameters used in their definition are given by:

the box size,

$$a_\alpha = |z_\alpha| y_{\alpha \mathrm{m}}/h, \tag{140}$$

the asymptotic channel momenta $k_\alpha^2 = (k_{\alpha 1}^2, \ldots k_{\alpha N}^2)$, where

$$k_{\alpha n}^2 = 2\left(E - z_\alpha^2 \varepsilon_n(a_\alpha)\right), \tag{141}$$

and the matrix of multipole couplings,

$$A_{\alpha n m}^{(\lambda)} = \frac{2V_\alpha^{(\lambda)}}{|z_\alpha|^\lambda} \int_0^{a_\alpha} \mathcal{B}_n(t;a_\alpha) t^\lambda \mathcal{B}_m(t;a_\alpha)\, dt. \tag{142}$$

It is usually sufficient to put Λ_α = 3-5. Expansion (139) must include all open channels ($k_{\alpha n}^2 > 0$) and several closed ones ($k_{\alpha n}^2 < 0$).

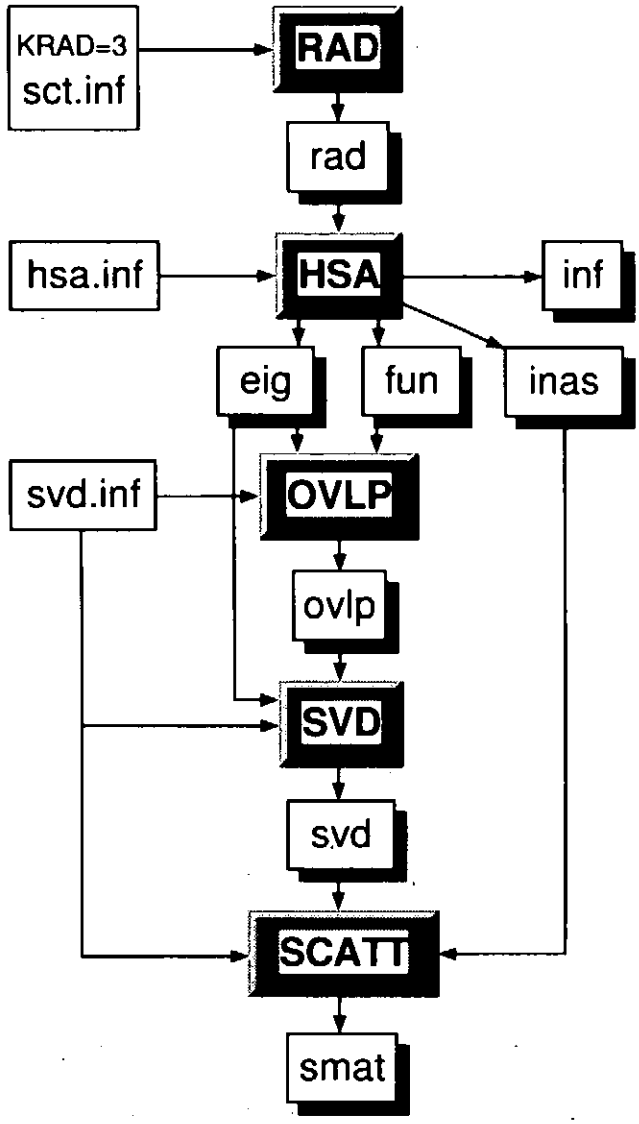

FIG. 5: CTBC executing sequence for scattering calculations.

3. Matching

Let $\Psi_{\nu_{\rm as}}(\mathbf{r})$ be a solution of Eq. (13) satisfying

$$\langle \Phi_\nu(\phi;r)|r^{-1/2}\Psi_{\nu_{\rm as}}(\mathbf{r})\rangle\big|_{r=r_{\rm m}} = \sum_\mu \mathcal{R}_{\nu\mu}\left\langle \Phi_\mu(\phi;r)\left|\frac{\partial r^{-1/2}\Psi_{\nu_{\rm as}}(\mathbf{r})}{\partial r}\right\rangle\right|_{r=r_{\rm m}} \tag{143}$$

and

$$\Psi_{\nu_{\rm as}}(\mathbf{r})|_{r\geq r_{\rm m}} = \tilde{\Psi}^{(s)}_{\nu_{\rm as}}(\mathbf{r}) + \sum_{\mu_{\rm as}} \tilde{\Psi}^{(c)}_{\mu_{\rm as}}(\mathbf{r}) K_{\mu_{\rm as}\nu_{\rm as}}. \tag{144}$$

Matching consists in the requirement that this function and its derivative with respect to r must coincide on both sides of the arc $r = r_{\rm m}$. Projecting these conditions on the HSA

TABLE I: User-supplied input information.

file	contents	description
sct.inf	N_r	dimension of radial DVR basis
	$N_{\rm sec}$	number of sectors
	$\bar{r}_k$, $k = 1, \ldots, N_{\rm sec}$	sector end points
hsa.inf	m_i, e_i, $i = 1, 2, 3$	masses and charges of particles
	σ	permutation symmetry (for symmetric case)
	N_ϕ	dimension of angular DVR basis
	$N_{\rm chmax} \leq N_\phi$	maximum number of HSA channels to be used in CTBC
svd.inf	$N_{\rm ch} \leq N_{\rm chmax}$	actual number of HSA channels
	E	energies for which scattering matrix is to be calculated

basis, we obtain

$$\mathbf{F}^{(s)} + \mathbf{F}^{(c)}\mathbf{K} = \mathcal{R}\left(\mathbf{D}^{(s)} + \mathbf{D}^{(c)}\mathbf{K}\right), \tag{145}$$

where

$$\mathbf{F}^{(s,c)}_{\nu\nu_{\rm as}} = \left\langle \Phi_\nu(\phi; r) | r^{-1/2} \tilde{\Psi}^{(s,c)}_{\nu_{\rm as}}(\mathbf{r}) \right\rangle \Big|_{r=r_{\rm m}}, \tag{146a}$$

$$\mathbf{D}^{(s,c)}_{\nu\nu_{\rm as}} = \left\langle \Phi_\mu(\phi; r) \left| \frac{\partial r^{-1/2} \tilde{\Psi}^{(s,c)}_{\nu_{\rm as}}(\mathbf{r})}{\partial r} \right\rangle \right|_{r=r_{\rm m}}. \tag{146b}$$

Matrix equation (145) is solved using singular value decomposition [17], which yields

$$\mathbf{K} = -\left(\mathbf{F}^{(c)} - \mathcal{R}\mathbf{D}^{(c)}\right)^{-1} \left(\mathbf{F}^{(s)} - \mathcal{R}\mathbf{D}^{(s)}\right). \tag{147}$$

The scattering matrix is then obtained from Eq. (61).

D. Structure of the program

The execution of the program proceeds in several steps, differently for bound state and scattering calculations. The program executing sequences and the organization of the information flow are illustrated in Figs. 4 and 5. There are three types of files: user-supplied input information, executables, and generated output results. Their contents and role are described in tables I-III.

TABLE II: Executables.

file	description
RAD	generates a set of radial points where HSA EVP (70) is to be solved
HSA	solves HSA EVP (70) and generates information needed to calculate matching integrals (146)
OVLP	calculates overlap matrices (99) and (110)
SVD	solves SVD EVP (96) in sectors
BOUND	calculates bound states
SCATT	calculates scattering matrix

TABLE III: Generated output results.

file	contents	description
rad	r_i	radial points
inf		HSA run information, an auxiliary file
eig	$U_\nu(r_i)$	HSA eigenvalues
fun	$\Phi_\nu(\phi; r_i)$	HSA eigenfunctions
inas	$\Phi_\nu(\phi; r_{\rm m})$, $\mathcal{B}_n(x;a)$, $d\mathcal{B}_n(x;a)/dx$	matching information
ovlp	$O_{i\nu,j\mu}$, $O^{a,b}_{\nu,j\mu}$	overlap matrices
svd	$\bar{E}_n$, $\bar{F}_{\nu n}(\bar{r}_k)$	SVD eigenvalues and surface amplitudes
beig	E_n	bound state energies
bfun	$F_{\nu n}(r_i)$	bound state radial functions
smat	$\mathbf{S}(E)$	scattering matrix

VI. ILLUSTRATIVE CALCULATIONS

Application of program CTBC is illustrated in Figs. 6-29, where results of calculations for a number of representative systems and processes are shown. HSA eigenvalues are represented by HSA potentials (81) and effective quantum numbers

$$n(r) = [-2U(r)]^{-1/2}. \tag{148}$$

Inelastic scattering processes are characterized by probabilities $p_{if} = |S_{if}|^2$ as functions of

$$n(E) = [-2E]^{-1/2}. \tag{149}$$

A. *epe*, $\sigma = +$ (case A)

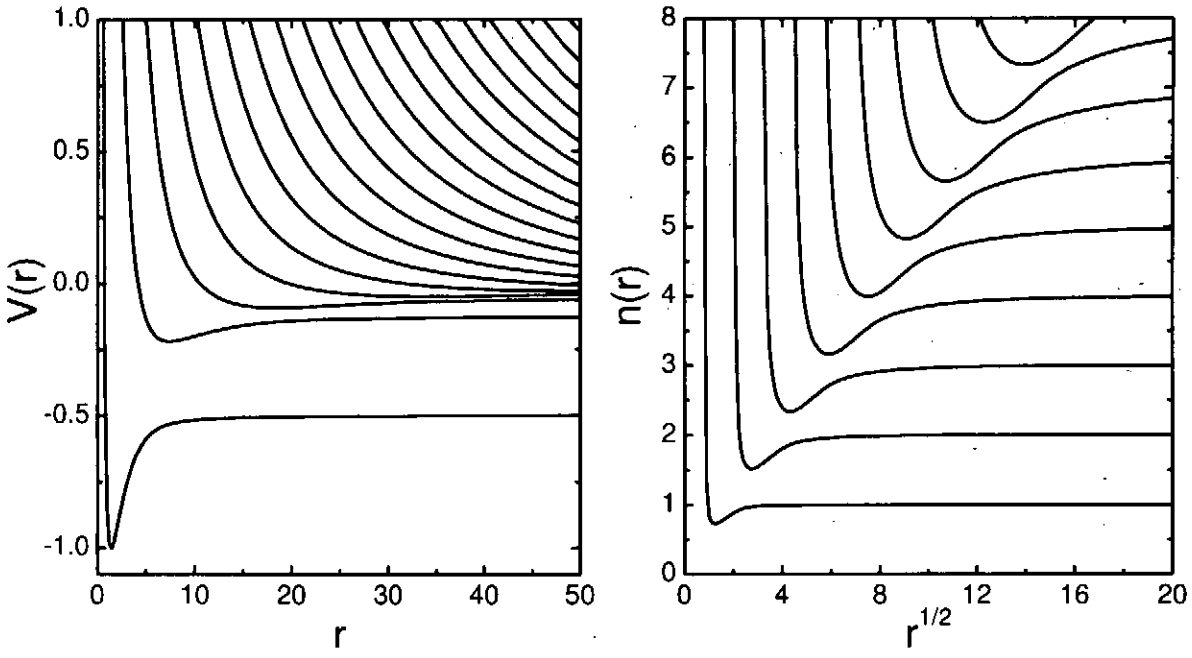

FIG. 6: HSA potentials for *epe*, $\sigma = +$. The ground state energy $E = -0.646\,598\,261$.

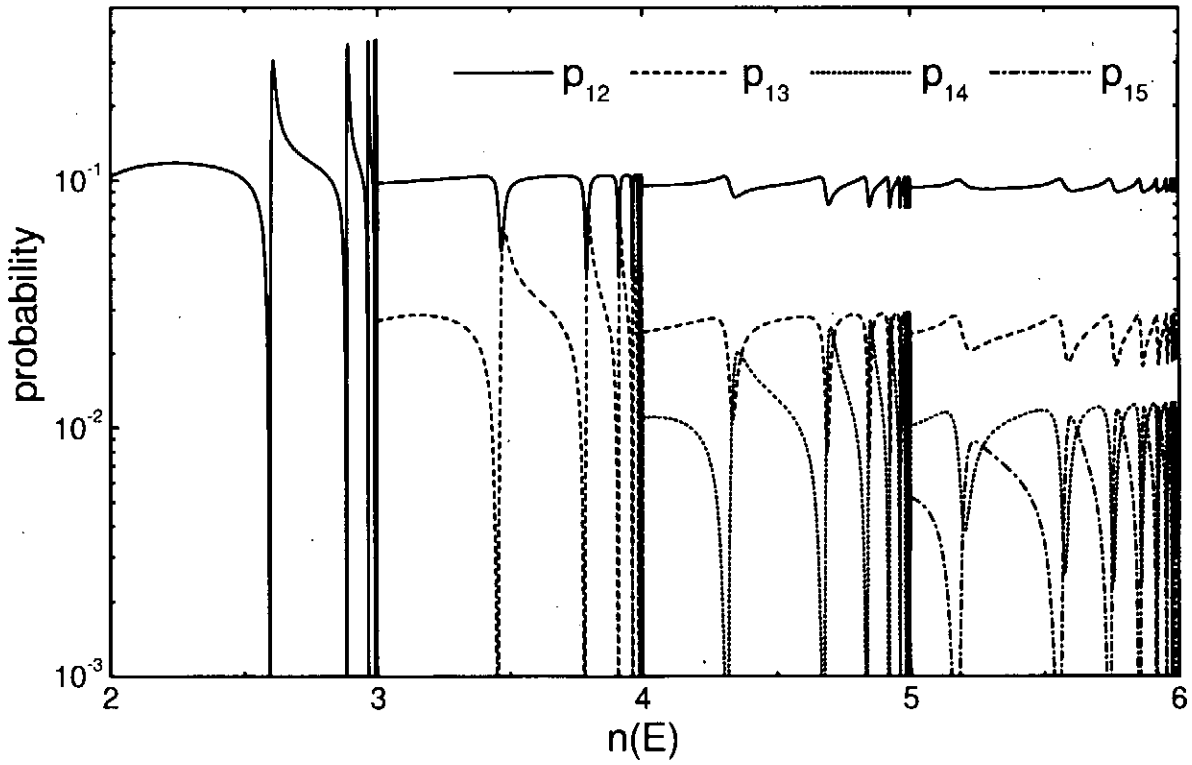

FIG. 7: Probabilities p_{1n} of $(ep)_1 + e \leftrightarrow (ep)_n + e$, $\sigma = +$.

B. *epe*, $\sigma = -$ **(case A)**

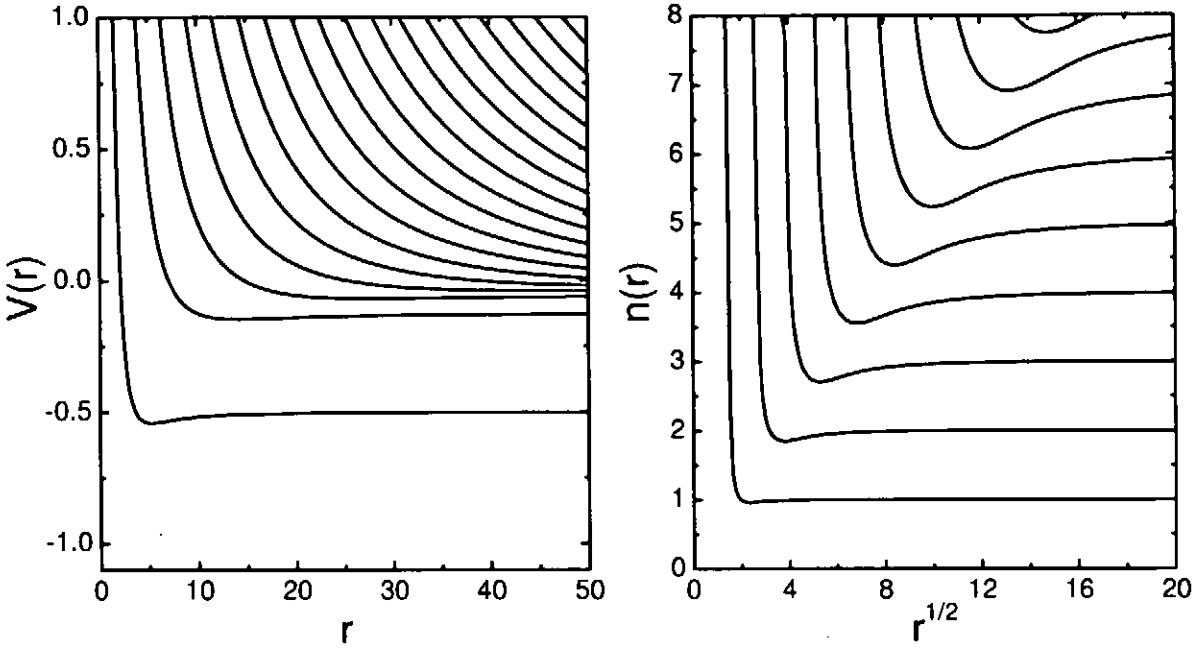

FIG. 8: HSA potentials for *epe*, $\sigma = -$. The ground state energy $E = -0.504\,154\,103$.

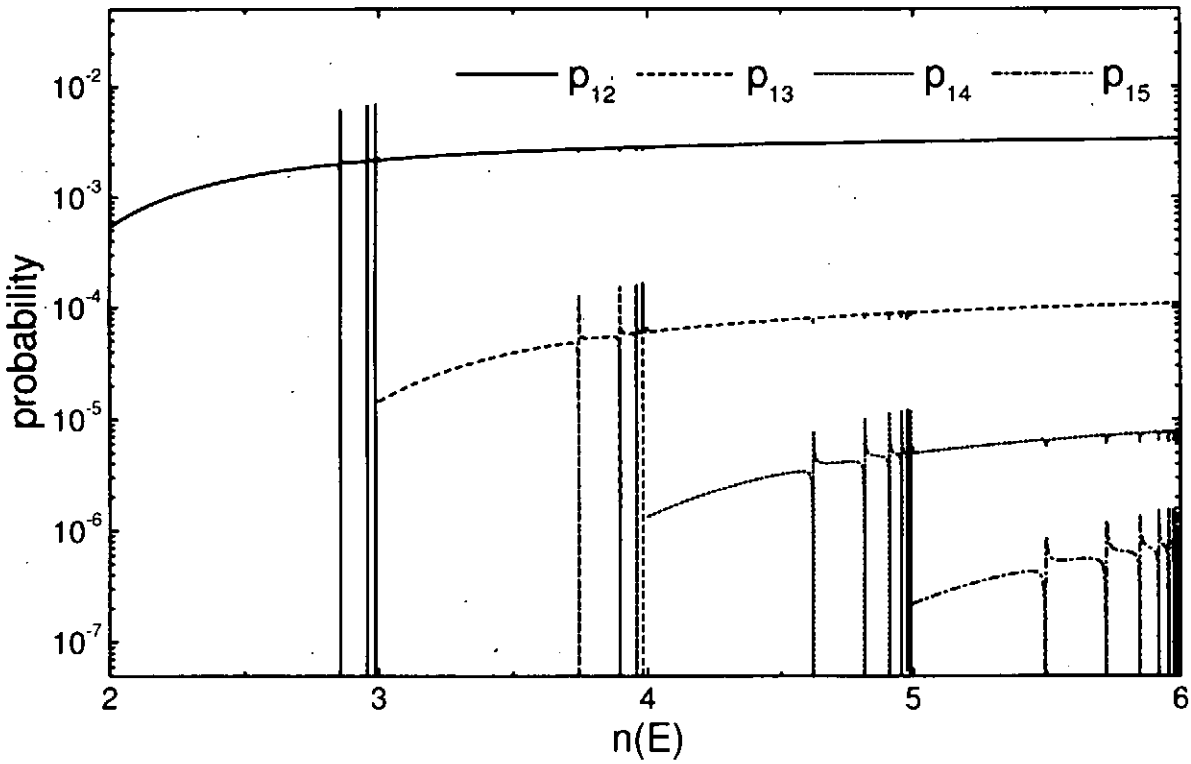

FIG. 9: Probabilities p_{1n} of $(ep)_1 + e \leftrightarrow (ep)_n + e$, $\sigma = -$.

C. *pee* (case B)

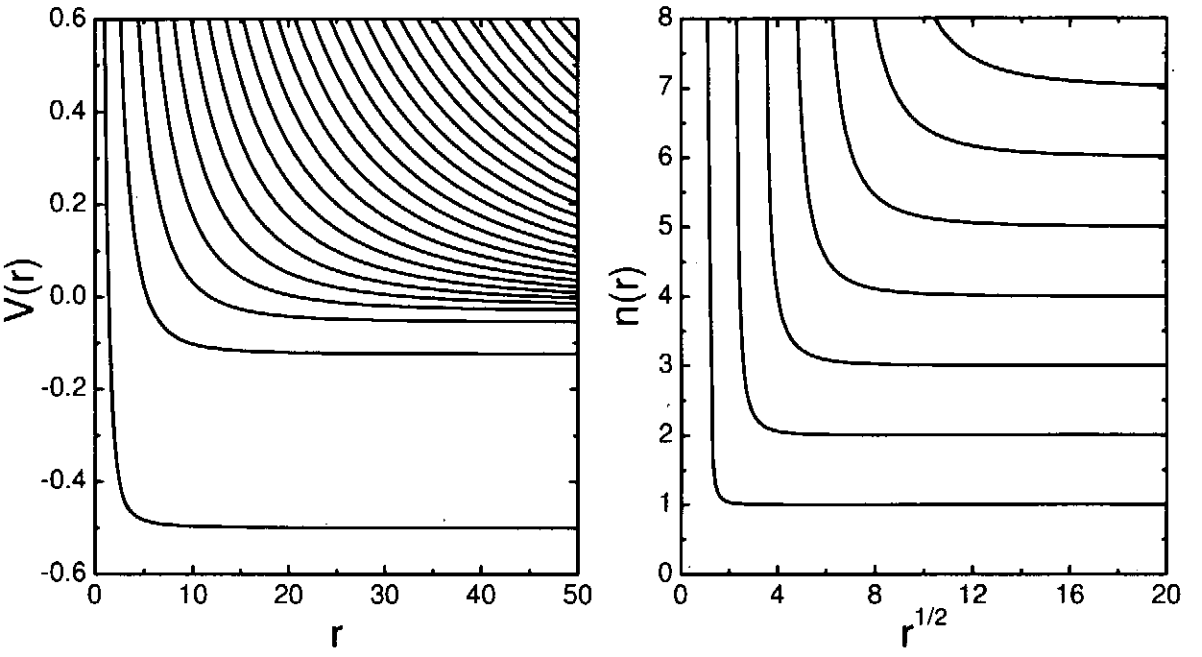

FIG. 10: HSA potentials for *pee*. There are no bound states in this system.

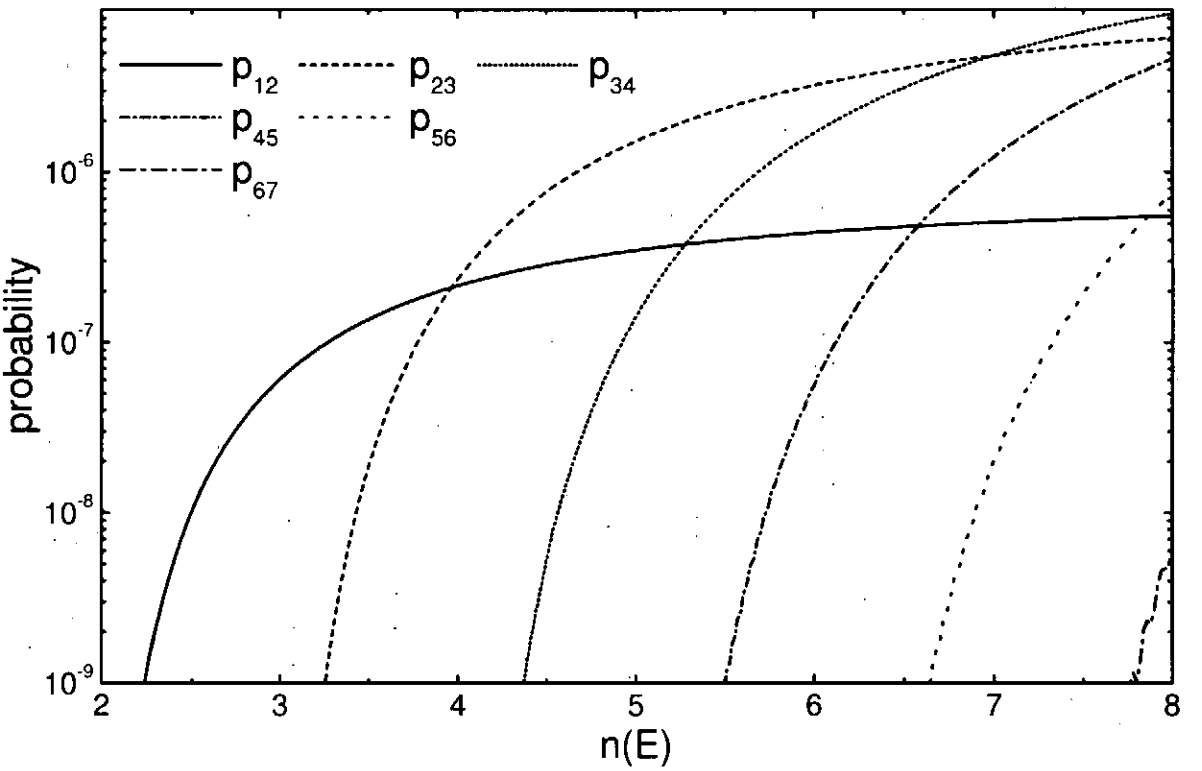

FIG. 11: Probabilities $p_{n\,n+1}$ of $(pe)_n + e \leftrightarrow (pe)_{n+1} + e$.

D. ee^+e, $\sigma = +$ (case A)

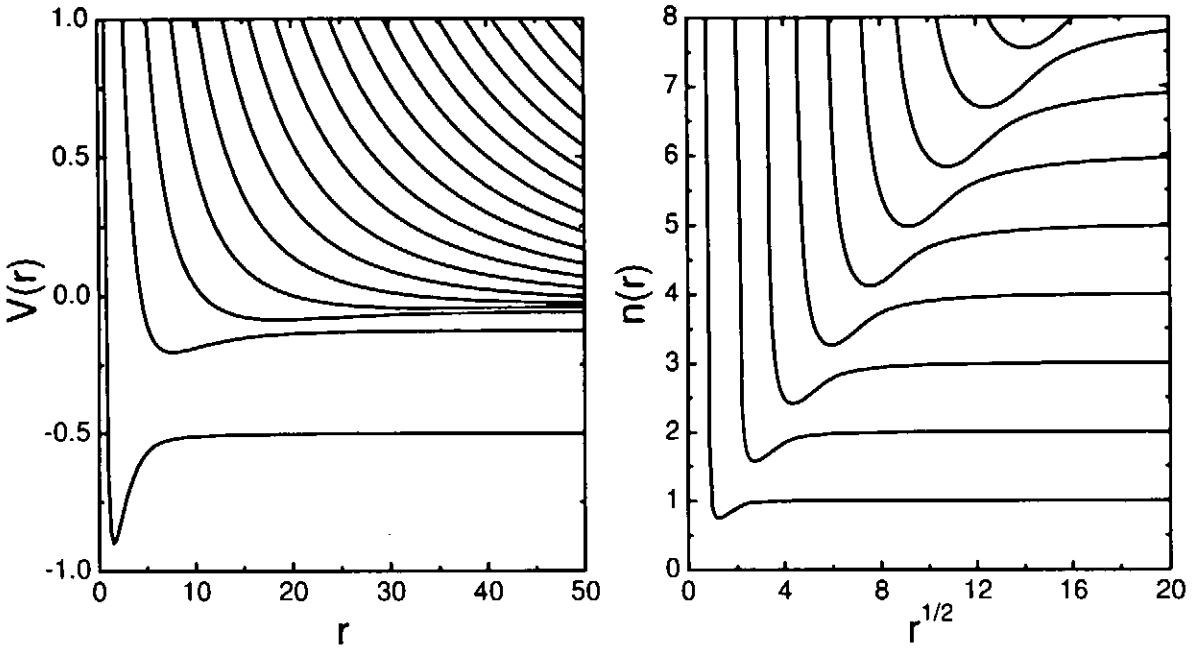

FIG. 12: HSA potentials for ee^+e, $\sigma = +$. The ground state energy $E = -0.674\,841\,185$.

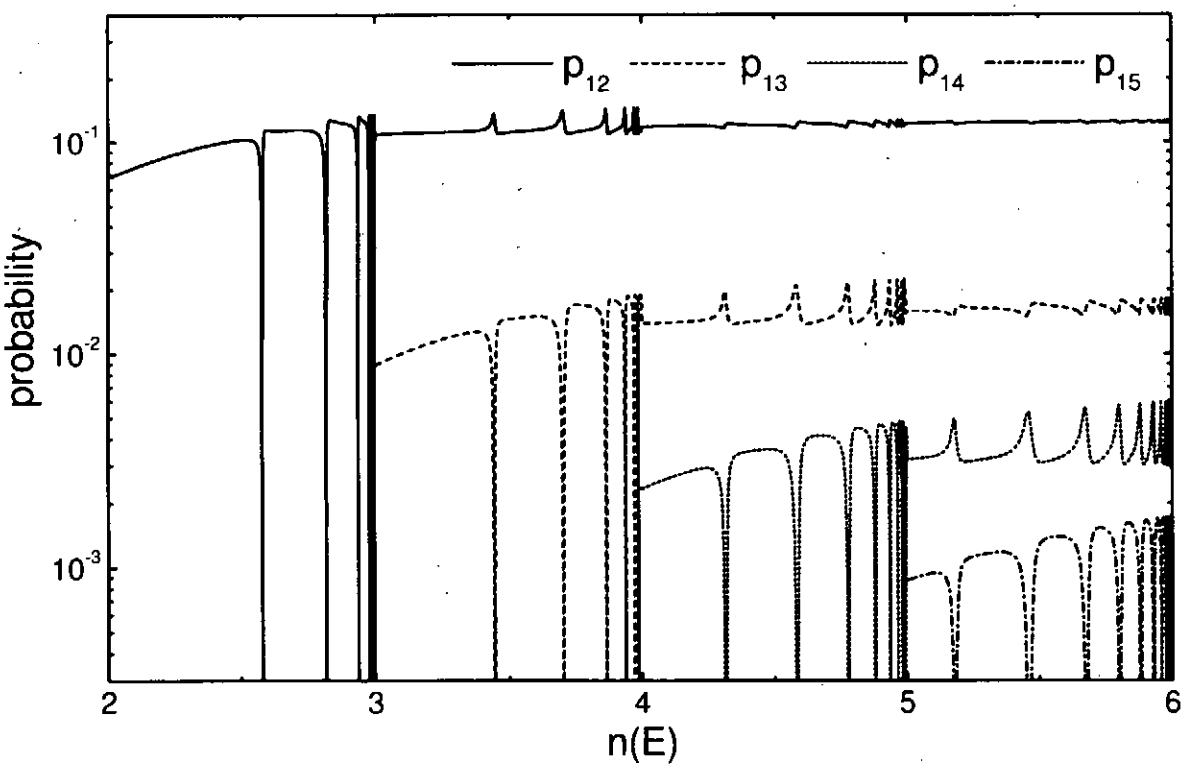

FIG. 13: Probabilities p_{1n} of $(ee^+)_1 + e \leftrightarrow (ee^+)_n + e$, $\sigma = +$.

E. ee^+e, $\sigma = -$ (case A)

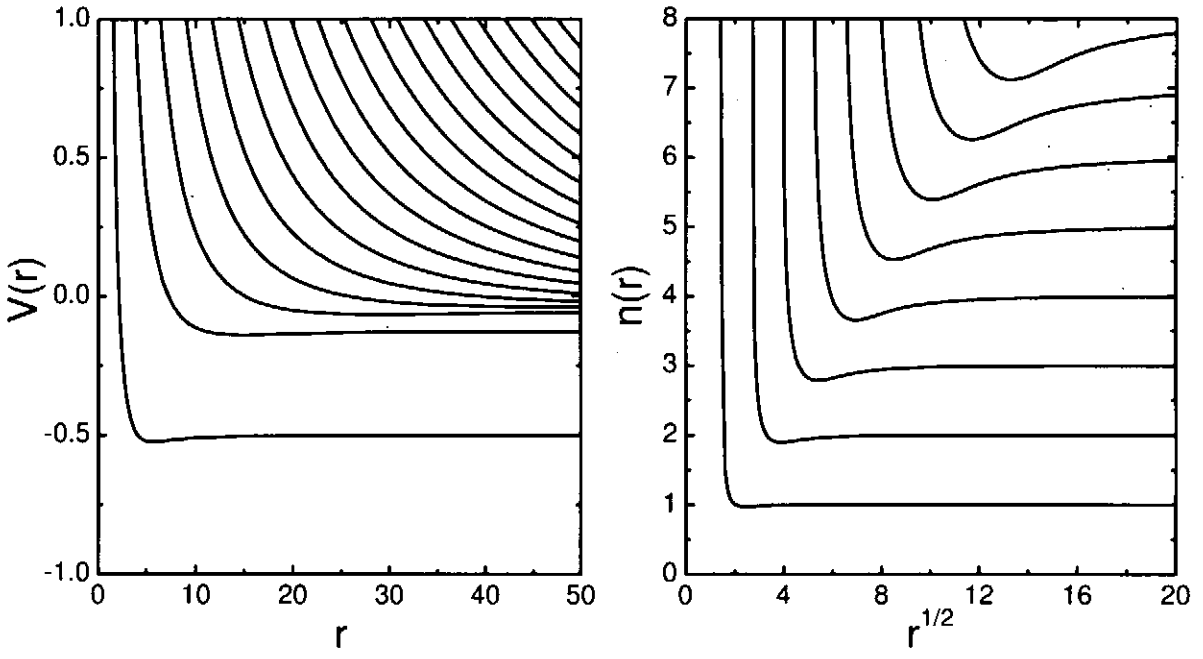

FIG. 14: HSA potentials for ee^+e, $\sigma = -$. The ground state energy $E = -0.504\,024\,113$.

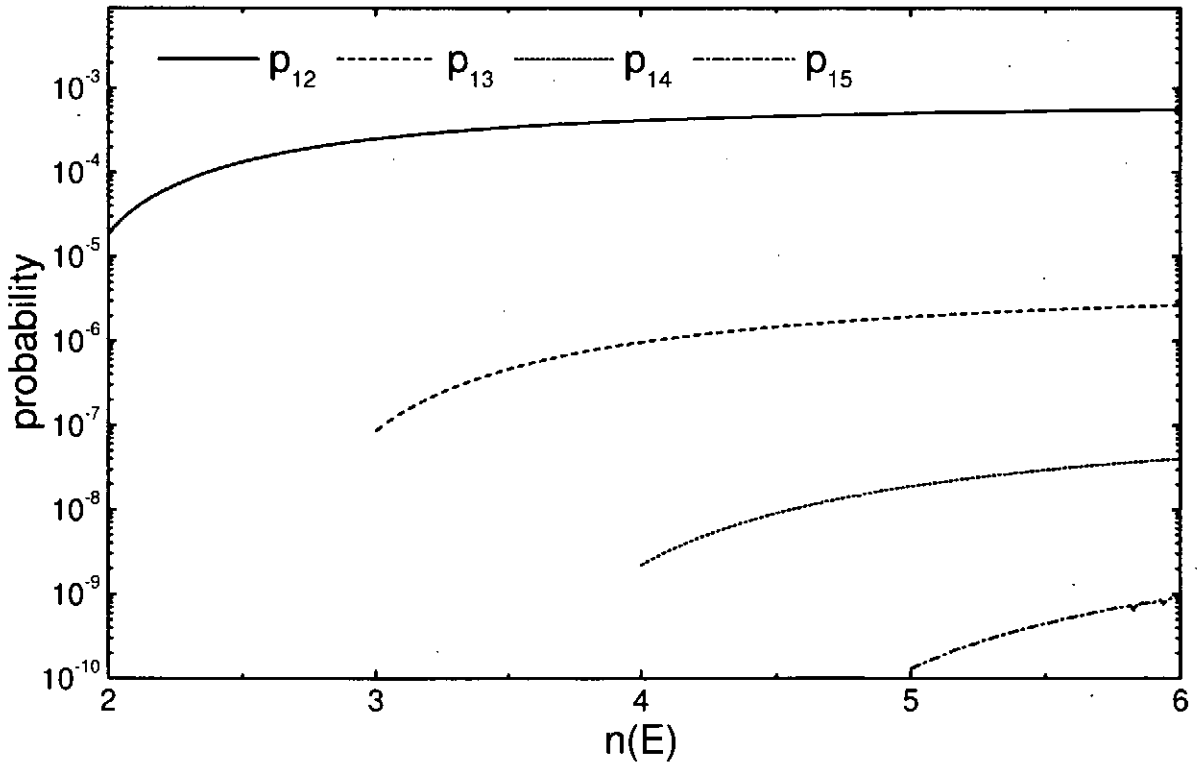

FIG. 15: Probabilities p_{1n} of $(ee^+)_1 + e \leftrightarrow (ee^+)_n + e$, $\sigma = -$. Resonances are not resolved.

F. e^+ee (case B)

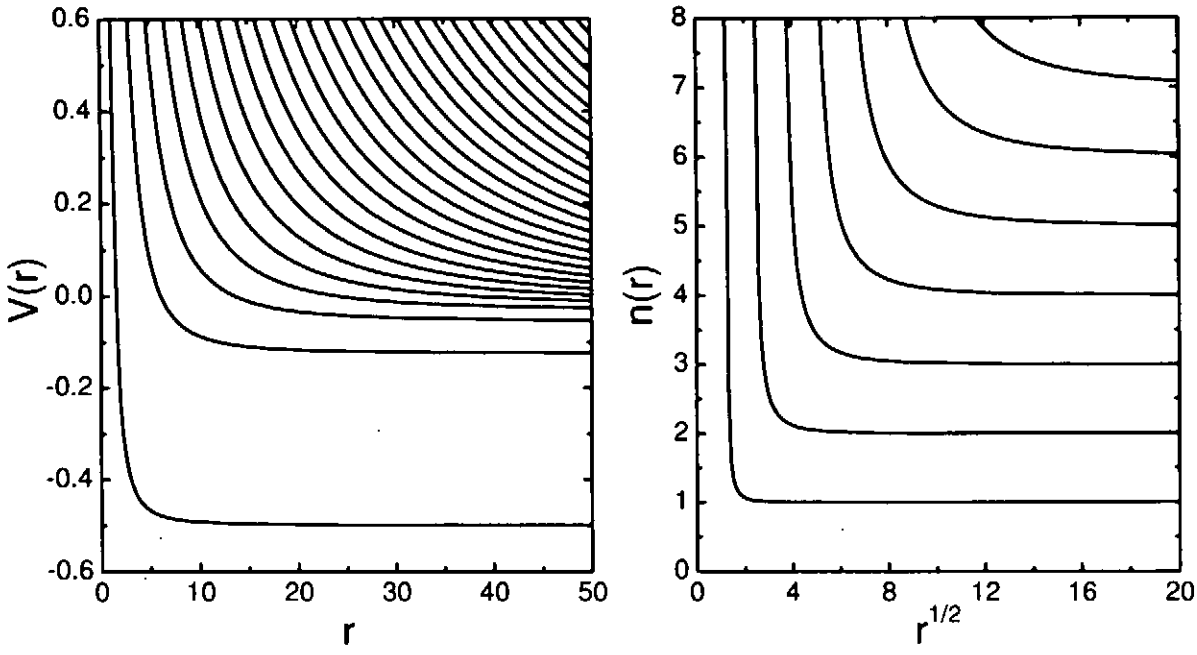

FIG. 16: HSA potentials for e^+ee. There are no bound states in this system.

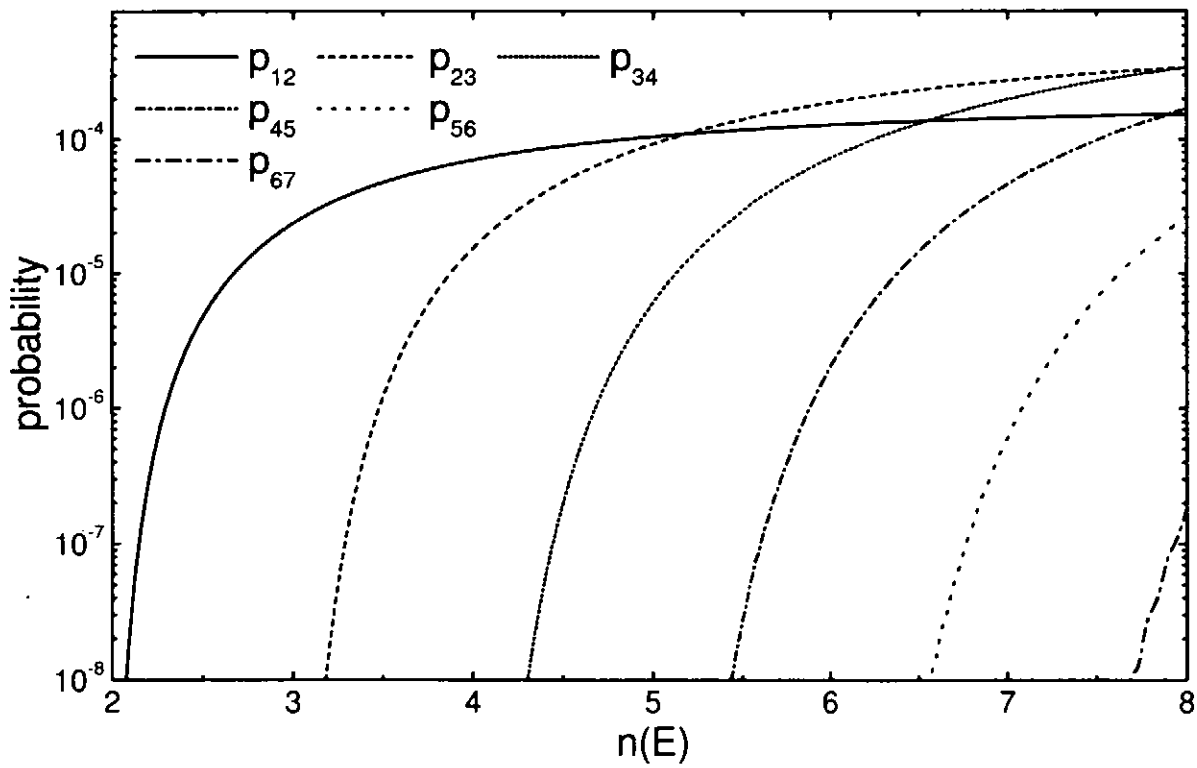

FIG. 17: Probabilities p_{nn+1} of $(e^+e)_n + e \leftrightarrow (e^+e)_{n+1} + e$.

G. pee^+ (case A)

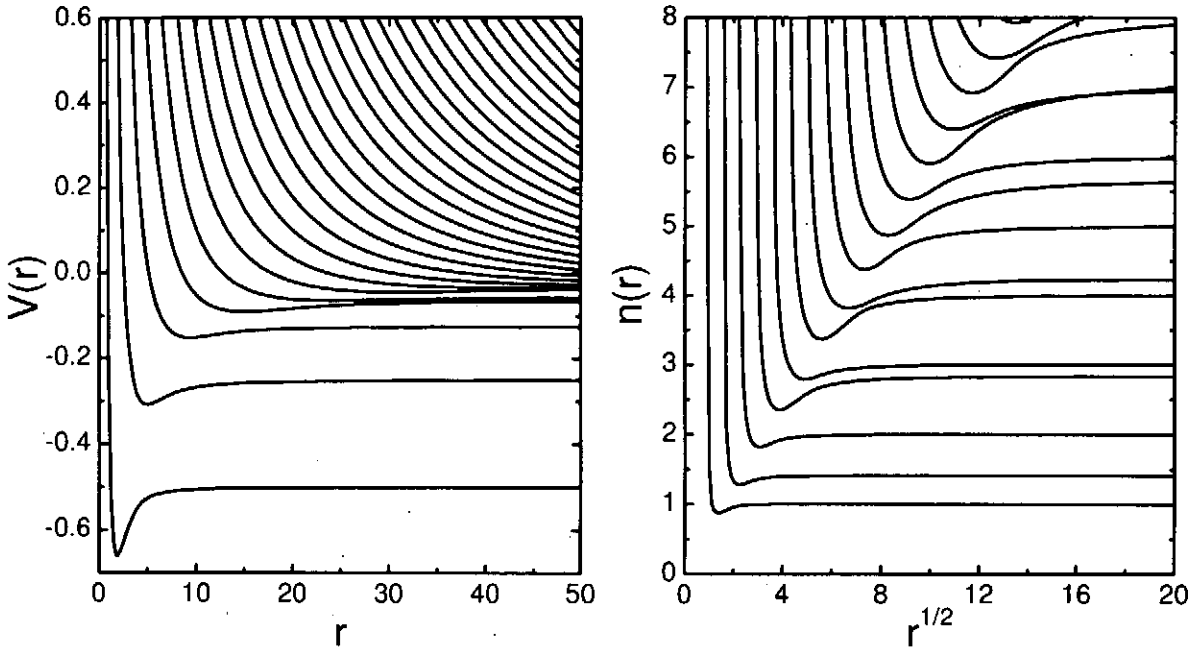

FIG. 18: HSA potentials for pee^+. The ground state energy $E = -0.550\,436\,989$.

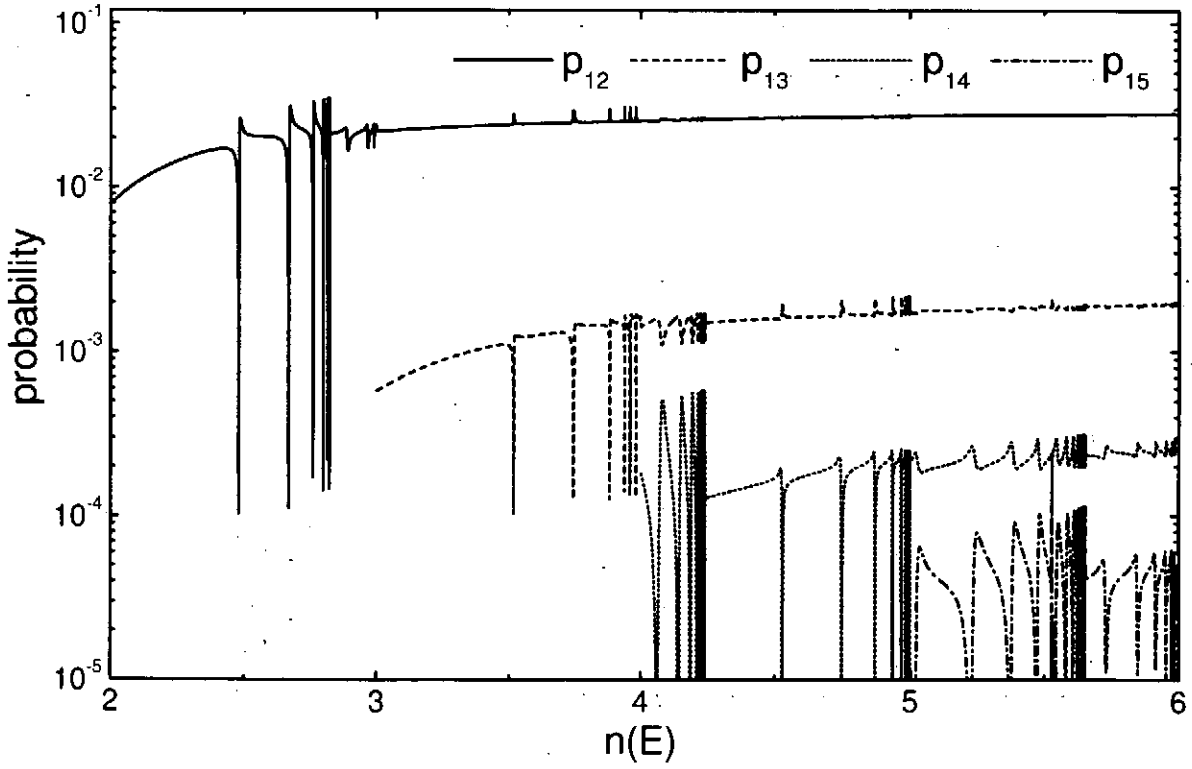

FIG. 19: Probabilities p_{1n} of $(pe)_1 + e^+ \leftrightarrow (pe)_n + e^+$.

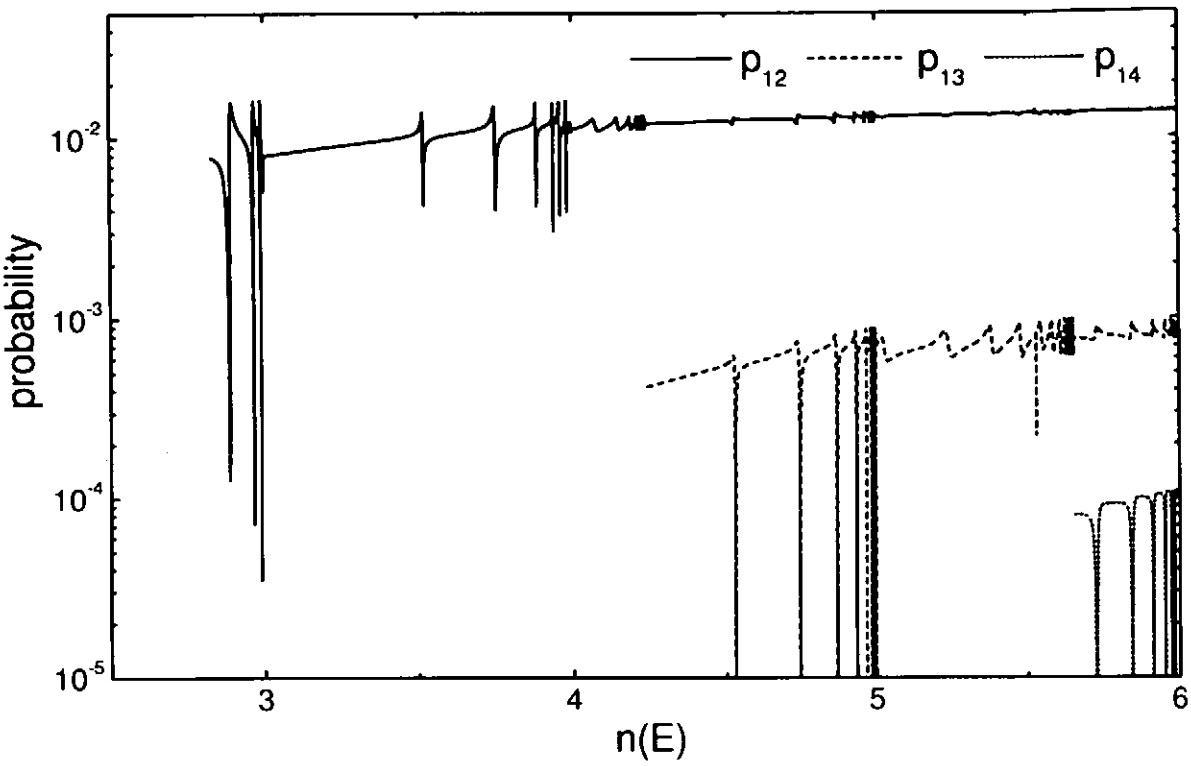

FIG. 20: Probabilities p_{1n} of $p + (ee^+)_1 \leftrightarrow p + (ee^+)_n$.

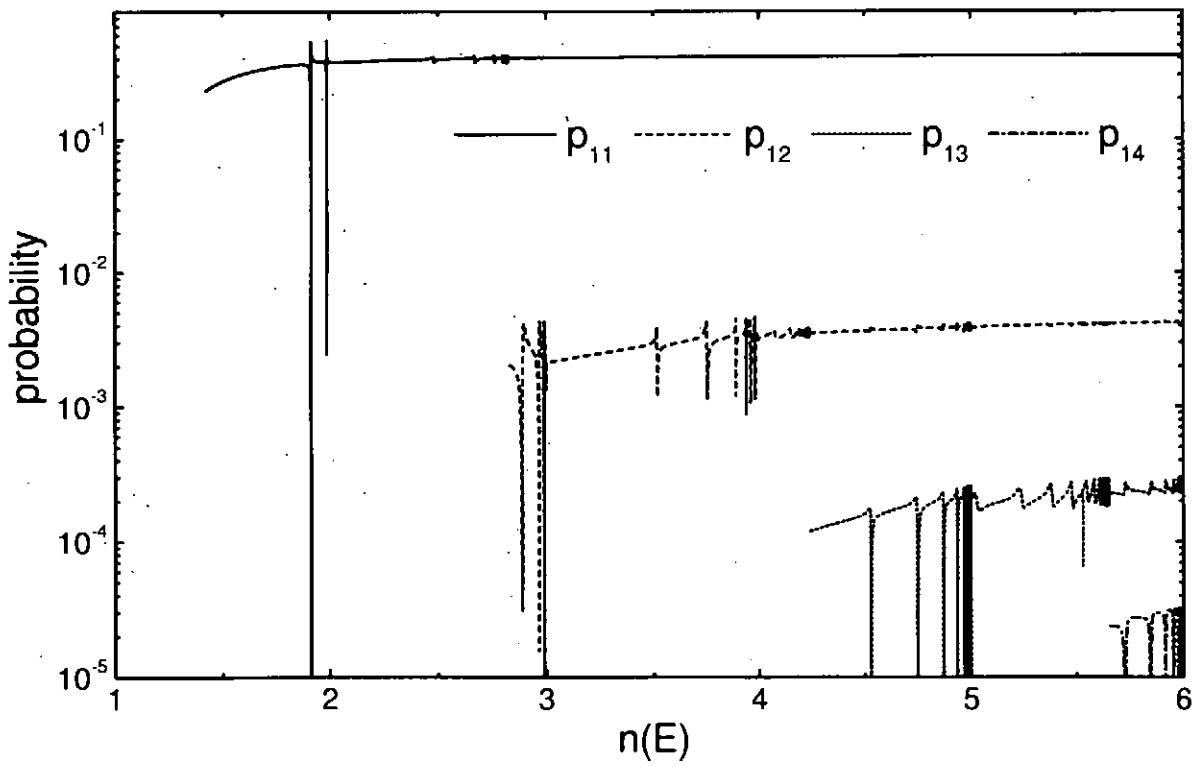

FIG. 21: Probabilities p_{1n} of $(pe)_1 + e^+ \leftrightarrow p + (ee^+)_n$.

H. epe^+ (case B1)

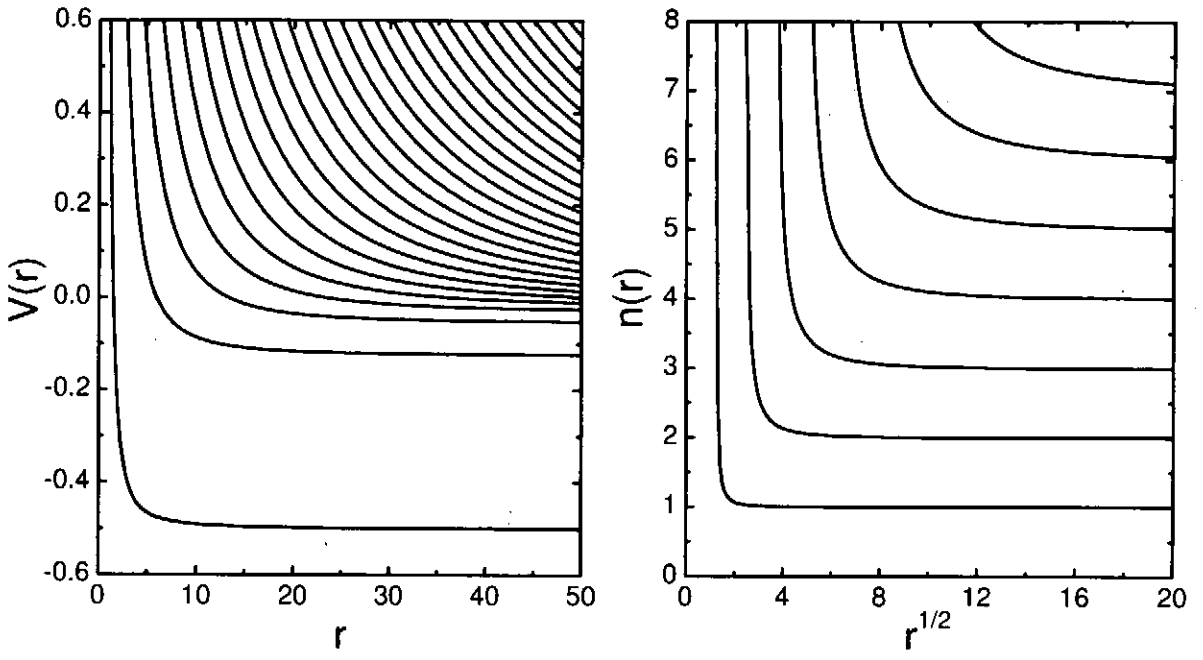

FIG. 22: HSA potentials for epe^+. There are no bound states in this system.

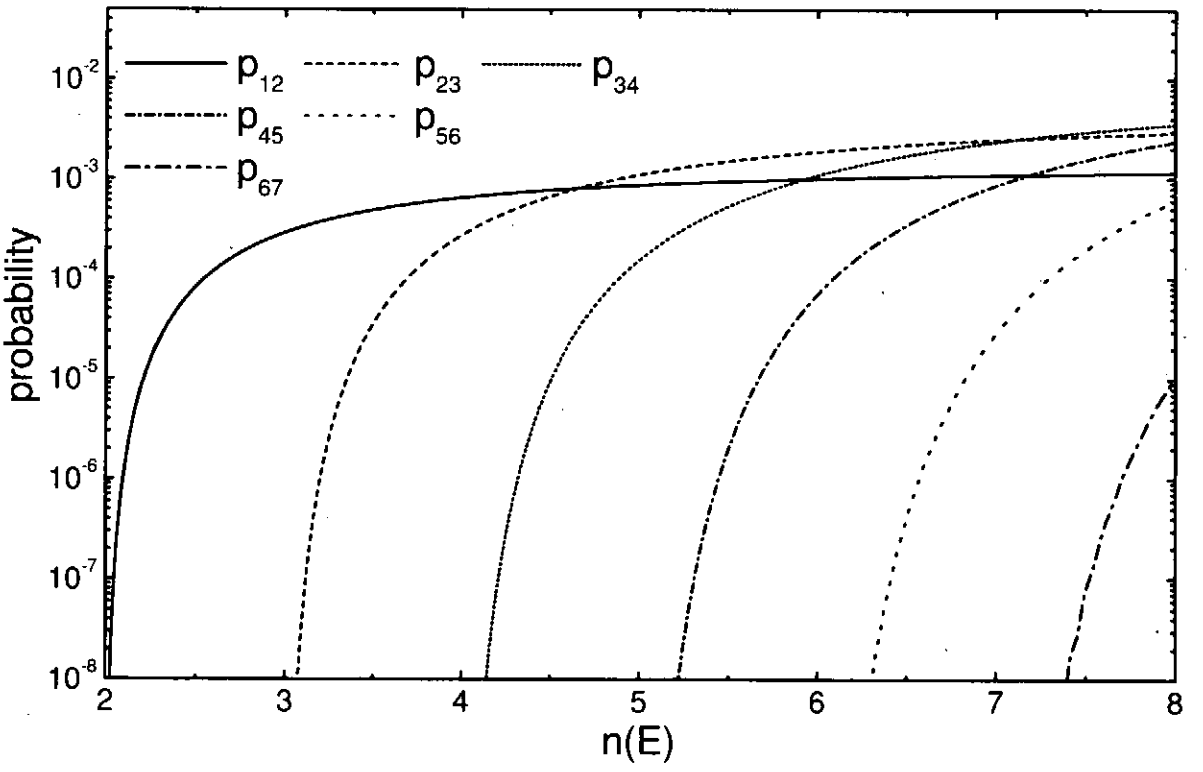

FIG. 23: Probabilities $p_{n\,n+1}$ of $(ep)_n + e^+ \leftrightarrow (ep)_{n+1} + e^+$.

I. ee^+p (case B2)

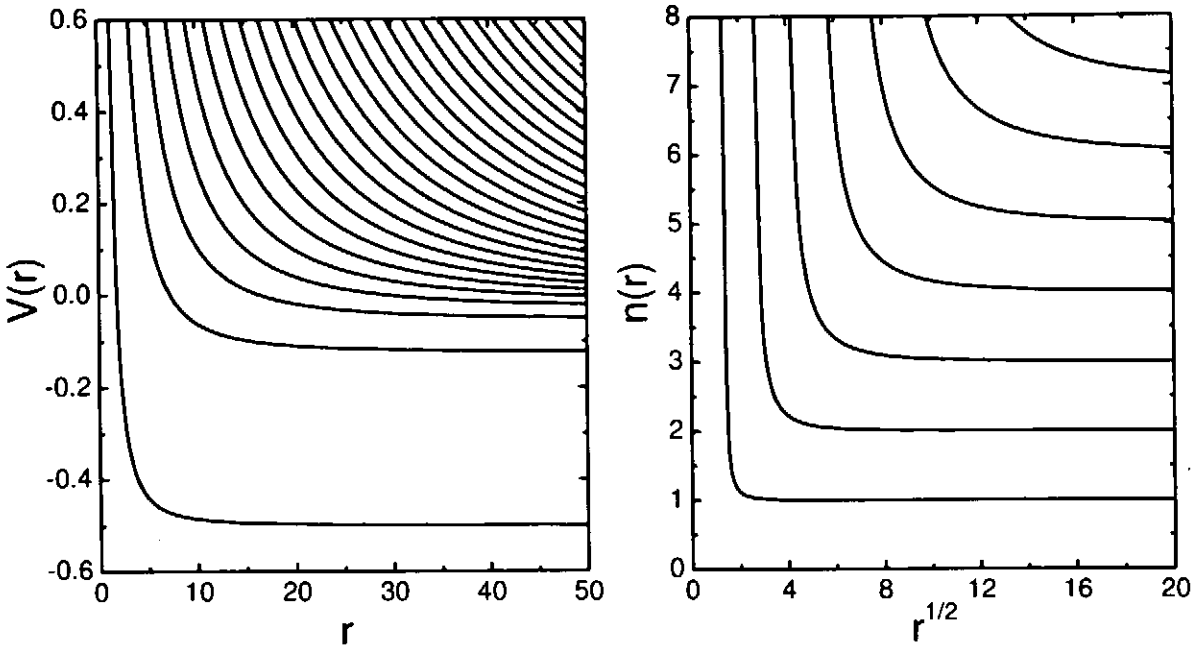

FIG. 24: HSA potentials for ee^+p. There are no bound states in this system.

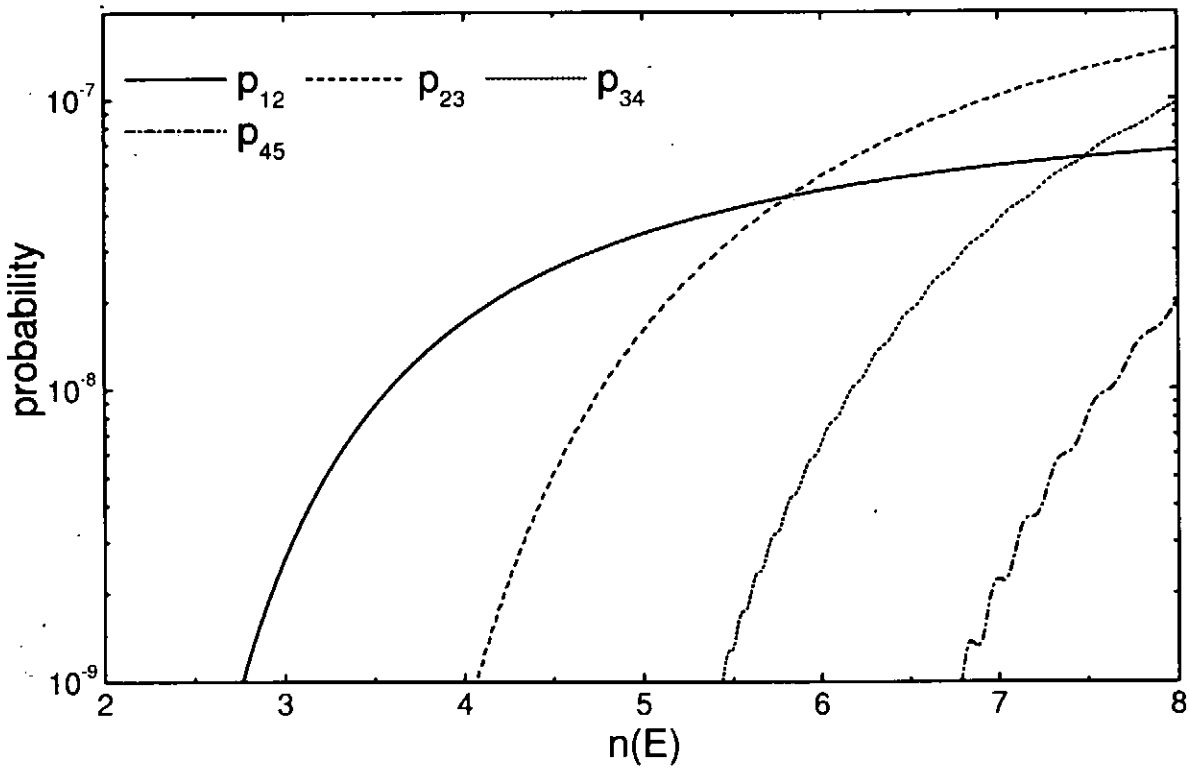

FIG. 25: Probabilities $p_{n\,n+1}$ of $(ee^+)_n + p \leftrightarrow (ee^+)_{n+1} + p$.

J. $t\mu d$ (case A)

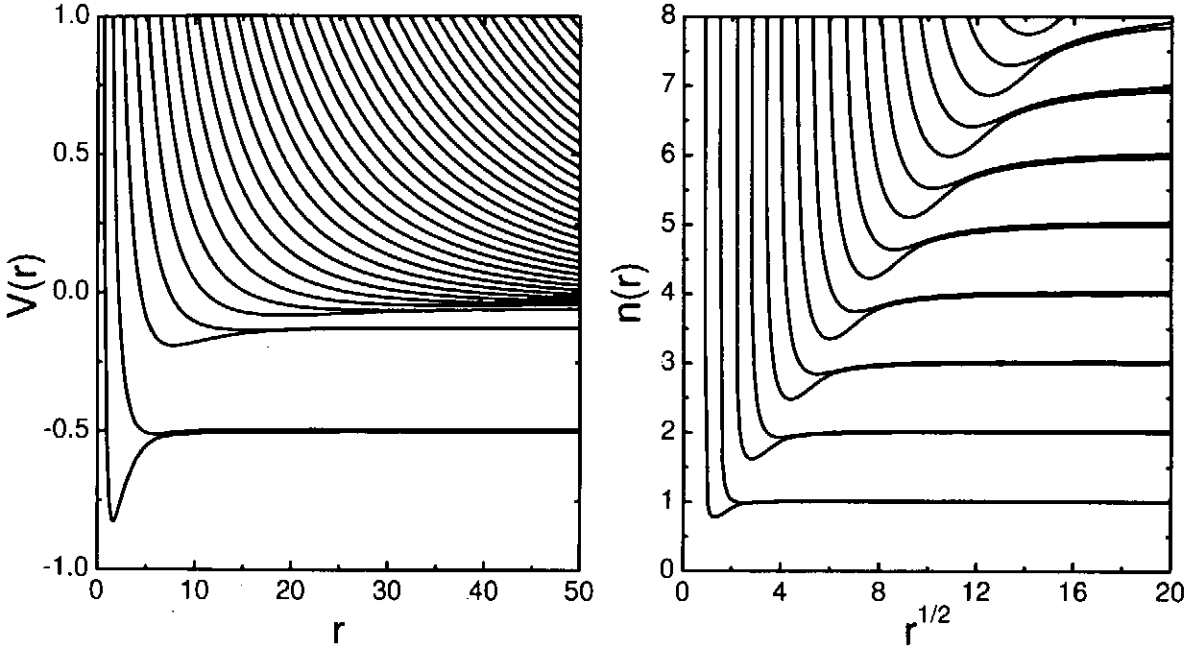

FIG. 26: HSA potentials for $t\mu d$. The ground state energy $E = -0.762\,627\,232$.

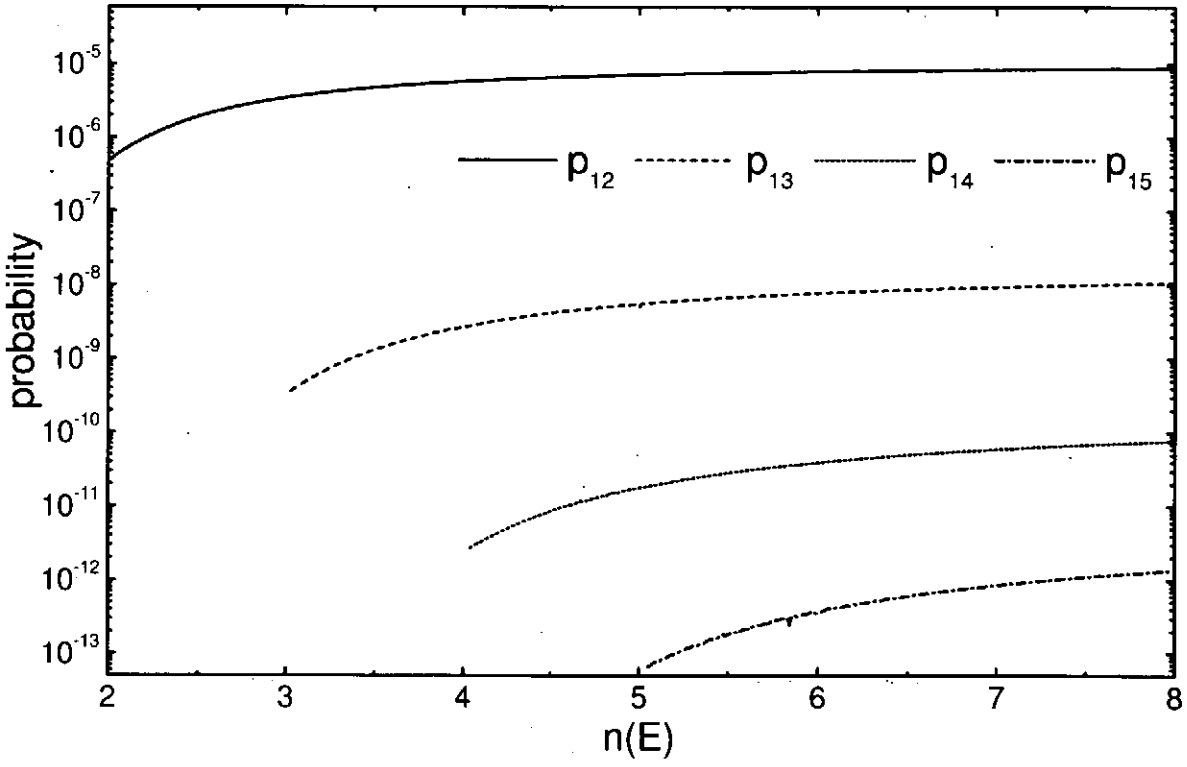

FIG. 27: Probabilities p_{1n} of $(t\mu)_1 + d \leftrightarrow (t\mu)_n + d$. Resonances are not resolved.

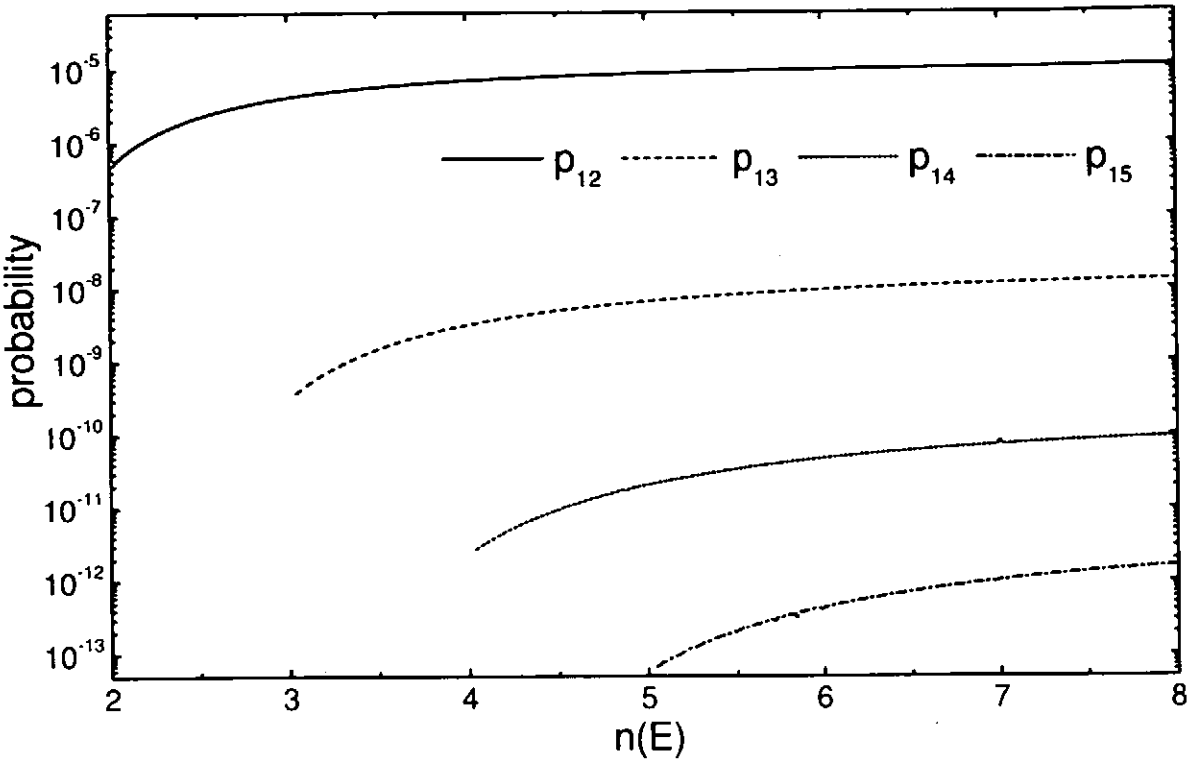

FIG. 28: Probabilities p_{1n} of $t + (\mu d)_1 \leftrightarrow t + (\mu d)_n$. Resonances are not resolved.

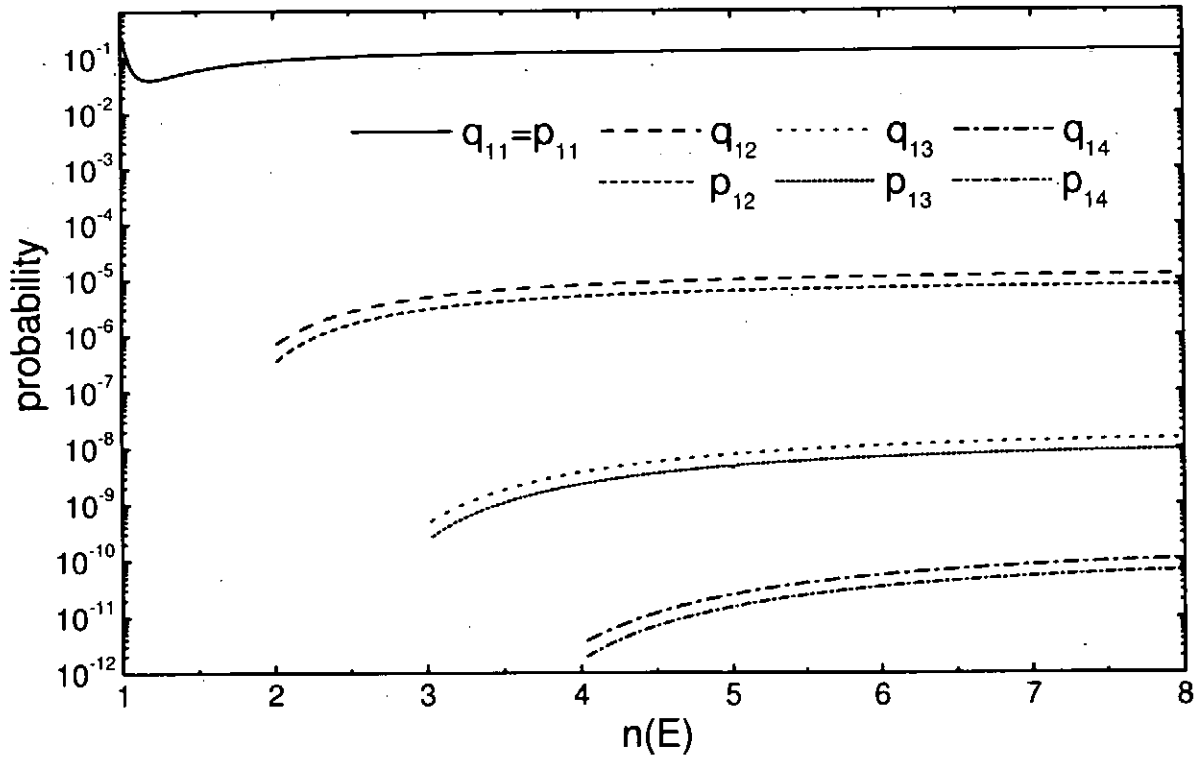

FIG. 29: Probabilities of $(t\mu)_1 + d \leftrightarrow t + (\mu d)_n$ and $t + (\mu d)_1 \leftrightarrow (t\mu)_n + d$, p_{1n} and q_{1n}, respectively. Resonances are not resolved.

The scattering results reported in Figs. 6-29 were obtained with $N_\phi = 250$, $N_{\rm ch} = 30$, sector size equal to $h\pi$, $N_r = 6$, and $r_{\rm m} = 3000$. The energy independent part of the calculations (modules RAD, HSA, OVLP, and SVD) took from 5 minutes for *epe* (a symmetric system with $h \approx 1$) to two hours for $t\mu d$ (a general system with $h \ll 1$). The energy dependent module SCATT took 10-30 seconds per one energy point. The main parameter controlling what could be calculated with the given set of energy independent information is the matching radius $r_{\rm m}$. In order to consider scattering processes in the near threshold energy regions as well as those involving highly excited states the parameter $r_{\rm m}$ must be sufficiently large; if it is not, then the calculated transition probabilities may have unphysical oscillations as in curve p_{45} in Fig. 25.

VII. CONCLUSIONS

Program CTBC provides a tool for studying the quantum dynamics of the collinear three-body Coulomb problem. However, the results obtained by this tool have the character of a virtual experiment rather than a theory, and another theory is required for their qualitative interpretation. For example, Figs. 6-29 show that probabilities of similar processes in systems with different masses of particles may differ by many orders of magnitude. Why it is so? What are the major mechanisms governing the dynamics? We believe the answers to these questions can be obtained by asymptotic methods. In order to appreciate the quality of the asymptotic results and hence the prediction power of the asymptotic theory, the accurate numerical information supplied by CTBC is indispensable.

Acknowledgments

O.I.T. thanks all members and technical staff of the Data and Planning Center, National Institute for Fusion Science, for hospitality during his stay at NIFS.

APPENDIX A: ASYMPTOTIC STATES

Asymptotic states in our problem are represented by products or linear combinations of products of two functions describing the internal state of a bound pair and the relative motion of the bound pair and a free particle, respectively, see Eqs. (54) and (139). Here we define these functions.

1. Bound-motion part

a. Hydrogenic states

Defining equation:

$$\left[-\frac{1}{2}\frac{d^2}{dx^2} - \frac{1}{x} - \varepsilon\right] \mathcal{B}(x) = 0, \tag{A1a}$$

$$\mathcal{B}(0) = \mathcal{B}(\infty) = 0. \tag{A1b}$$

The solutions are given by

$$\varepsilon_n = -\frac{1}{2n^2}, \quad \mathcal{B}_n(x) = \frac{2x}{n^2}\, e^{-x/n} \tilde{L}^{(1)}_{n-1}(2x/n), \qquad n = 1, 2, \ldots, \tag{A2}$$

where $\tilde{L}^{(\alpha)}_n(x)$ are normalized Laguerre polynomials [15]. Functions $\mathcal{B}_n(x)$ satisfy

$$\int_0^\infty \mathcal{B}_n(x)\mathcal{B}_m(x)\, dx = \delta_{nm}. \tag{A3}$$

Their derivatives are given by

$$\frac{d\mathcal{B}_n(x)}{dx} = \frac{1}{n^{3/2}}\, e^{-x/n} \left[\sqrt{n+1}\, \tilde{L}^{(1)}_n(2x/n) - \sqrt{n-1}\, \tilde{L}^{(1)}_{n-2}(2x/n)\right]. \tag{A4}$$

Using the relation [15]

$$\tilde{L}^{(\alpha)}_n(ax) = \sum_{k=0}^{n} \sqrt{\frac{n!\Gamma(n+\alpha+1)}{k!\Gamma(k+\alpha+1)}}\, \frac{a^k(1-a)^{n-k}}{(n-k)!}\, \tilde{L}^{(\alpha)}_k(x), \tag{A5}$$

various matrix elements can be calculated. For example,

$$\int_0^\infty \mathcal{B}_n(x) x^{-1} \mathcal{B}_m(x)\, dx = \frac{4\sqrt{nm}(n-1)!(m-1)!}{(n+m)^{n+m}} \times \sum_{k=0}^{\kappa} (-1)^{\kappa-k} \frac{(4nm)^k |n-m|^{n+m-2k-2}}{k!(k+1)!(n-k-1)!(m-k-1)!}, \tag{A6}$$

where $\kappa = \min(n, m) - 1$. In particular, $(x^{-1})_{nn} = n^{-2}$.

b. Hydrogenic states in a box

Defining equation:

$$\left[-\frac{1}{2}\frac{d^2}{dx^2} - \frac{1}{x} - \varepsilon(a)\right] \mathcal{B}(x;a) = 0, \tag{A7a}$$

$$\mathcal{B}(0;a) = \mathcal{B}(a;a) = 0, \tag{A7b}$$

where a is the box size. Introduce a new variable,

$$\begin{array}{c} x(t) = a(1+t)/2, \\ 0 \le x \le a, \end{array} \quad \leftrightarrow \quad \begin{array}{c} t(x) = 2x/a - 1, \\ -1 \le t \le 1, \end{array} \tag{A8}$$

and rewrite Eq. (A7) in the standard form (B23),

$$\left[\frac{d}{dt}(1-t^2)\frac{d}{dt} - \frac{1}{1-t^2} + \frac{a^2}{2}(1-t^2)\left(\varepsilon(a) + \frac{2}{a(1+t)}\right)\right] \frac{\mathcal{B}(x;a)}{\sqrt{1-t^2}} = 0. \tag{A9}$$

This equation is solved numerically by the DVR method using N-point Jacobi $P_n^{(1,1)}(t)$ quadrature, see appendix B. The solutions are obtained in the form

$$\varepsilon_n(a), \quad \mathcal{B}_n(x;a) = \left(\frac{2}{a}\right)^{1/2} \sqrt{1-t^2} \sum_{i=1}^{N} \frac{c_i^n}{\sqrt{1-t_i^2}} \pi_i(t), \qquad n = 1, 2, \ldots, N. \tag{A10}$$

The eigenvectors c_i^n are normalized by

$$\sum_{i=1}^{N} c_i^n c_i^m = \delta_{nm}. \tag{A11}$$

Then functions $\mathcal{B}_n(x;a)$ satisfy

$$\int_0^a \mathcal{B}_n(x;a)\mathcal{B}_m(x;a)\,dx \approx \delta_{nm}, \tag{A12}$$

where the approximation amounts to the use of quadrature (B7). They can be represented in terms of polynomials

$$\mathcal{B}_n(x;a) = (1-t^2)\sum_{k=1}^{N} f_k^n \tilde{P}_{k-1}^{(1,1)}(t), \tag{A13}$$

where

$$f_k^n = \left(\frac{2}{a}\right)^{1/2} \sum_{i=1}^{N} \frac{c_i^n T_{ki}}{\sqrt{1-t_i^2}}. \tag{A14}$$

Using the relation

$$\frac{d}{dt}\left[(1-t^2)\tilde{P}_{k-1}^{(1,1)}(t)\right] = p_k \tilde{P}_{k-2}^{(1,1)}(t) - p_{k+1}\tilde{P}_k^{(1,1)}(t), \tag{A15}$$

where

$$p_k = k\sqrt{\frac{k^2-1}{4k^2-1}}, \tag{A16}$$

their derivatives are given by

$$\frac{\mathcal{B}_n(x;a)}{dx} = \sum_{k=1}^{N+1} d_k^n \tilde{P}_{k-1}^{(1,1)}(t), \tag{A17}$$

where

$$d_k^n = \frac{2}{a}\left(p_{k+1} f_{k+1}^n - p_k f_{k-1}^n\right) \tag{A18}$$

and it is understood that $f_0^n = f_{N+1}^n = f_{N+2}^n = 0$. The matrix elements required for calculating multipole couplings (142) are given by

$$\int_0^a \mathcal{B}_n(x;a) x^\lambda \mathcal{B}_m(x;a)\, dx \approx (a/2)^\lambda \sum_{i=1}^{N} c_i^n (1+t_i)^\lambda c_i^m. \tag{A19}$$

Equation (A7) is a typical EVP arising in atomic physics. Let us use it as an example to demonstrate efficiency of the DVR method. The accuracy of eigenvalues $\varepsilon_n(a)$ obtained by this method as a function of the box size a, state n, and basis dimension N is illustrated in Fig. 30. For small a, function $\mathcal{B}_n(x;a)$ has similar amplitude all over the interval $0 \le x \le a$.

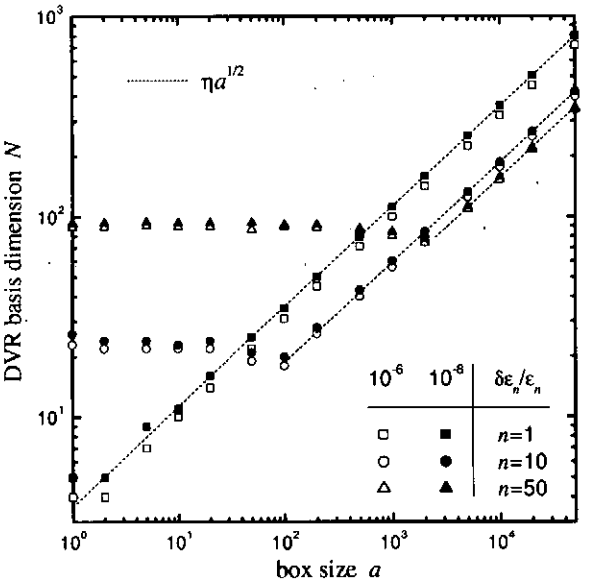

FIG. 30: The minimum dimension of DVR basis N which ensures the specified relative accuracy of eigenvalues $\varepsilon_n(a)$ as a function of the box size a for three representative states $n = 1$, 10, 50.

The minimum N which ensures the required accuracy of $\varepsilon_n(a)$ in this case does not depend on a and is proportional to n with the coefficient about 2. For large a, function $\mathcal{B}_n(x;a)$ is localized in a small interval of x near $x=0$ whose size vanishes as n^2/a, while the position of its first zero does not depend on n and can be estimated as $1/a$. In order to obtain an accurate solution, the interval between $x=0$ and the first zero of $\mathcal{B}_n(x;a)$ must contain several quadrature points. Taking into account that for $N\to\infty$ the first point x_1 of the Jacobi quadrature satisfies $(1-x_1)\propto 1/N^2$, we obtain the relation

$$N=\eta\sqrt{a}. \tag{A20}$$

The coefficient η here depends on state and the accuracy required. The localization problem is most severe for the lowest state $n=1$, see Fig. 30. We have found from numerical calculations the following dependence between η and the relative accuracy of $\varepsilon_1(a)$,

$$\eta=3.19\ \rightarrow\ \delta\varepsilon_1/\varepsilon_1<10^{-6}, \tag{A21a}$$

$$\eta=3.56\ \rightarrow\ \delta\varepsilon_1/\varepsilon_1<10^{-8}. \tag{A21b}$$

Equations (A20) and (A21) were checked in the interval $10\le a\le 5\times 10^4$.

2. Free-motion part

a. Coulomb wave

Defining equation for an open channel:

$$\left[\frac{d^2}{dx^2}-\frac{2\eta}{x}+1\right]\mathcal{F}(x;\eta)=0, \tag{A22a}$$

$$\mathcal{F}(x;\eta)|_{x\to\infty}=\exp\left[ix-i\eta\ln(2x)+i\delta\right], \tag{A22b}$$

where

$$\delta=\arg\Gamma(1+i\eta). \tag{A23}$$

The solution is given by

$$\mathcal{F}(x;\eta)=-2ie^{\pi\eta/2+i\delta}\times xe^{ix}U(1+i\eta,2,-2ix), \tag{A24}$$

where $U(a,b,x)$ is a confluent hypergeometric function [15]. The regular (s) and irregular (c) at $x=0$ solutions are given by

$$\begin{aligned}\mathcal{F}^{(s)}(x;\eta)=\mathrm{Im}\,\mathcal{F}(x;\eta)\ &\stackrel{x\to\infty}{\longrightarrow}\ \sin\left[x-\eta\ln(2x)+\delta\right],\\ \mathcal{F}^{(c)}(x;\eta)=\mathrm{Re}\,\mathcal{F}(x;\eta)\ &\stackrel{x\to\infty}{\longrightarrow}\ \cos\left[x-\eta\ln(2x)+\delta\right].\end{aligned} \tag{A25}$$

For $\eta = 0$ we have

$$\mathcal{F}(x;0) = e^{ix} \quad \Rightarrow \quad \begin{cases} \mathcal{F}^{(s)}(x;0) = \sin x, \\ \mathcal{F}^{(c)}(x;0) = \cos x. \end{cases} \tag{A26}$$

For a closed channel, only irregular solution is needed. It is defined by

$$\left[\frac{d^2}{dx^2} - \frac{2\eta}{x} - 1\right] \mathcal{F}^{(c)}(x;\eta) = 0, \tag{A27a}$$

$$\mathcal{F}^{(c)}(x;\eta)\big|_{x\to\infty} = \exp\left[-x - \eta \ln(2x)\right]. \tag{A27b}$$

The solution is given by

$$\mathcal{F}^{(c)}(x;\eta) = 2 \times x e^{-x} U(1+\eta, 2, 2x). \tag{A28}$$

For $\eta = 0$ we have

$$\mathcal{F}^{(c)}(x) = e^{-x}. \tag{A29}$$

b. Multichannel Coulomb wave with multipole couplings

Defining equation:

$$\left[\frac{d^2}{dx^2} - \frac{2Z}{x} + k_n^2\right] \mathcal{F}_n(x) = \sum_{m=1}^{N} \sum_{\lambda=1}^{\Lambda} \frac{A_{nm}^{(\lambda)}}{x^{\lambda+1}} \mathcal{F}_m(x), \quad n = 1, \ldots, N. \tag{A30}$$

For open channels, $k_n^2 > 0$, the regular (s) and irregular (c) solutions are defined by

$$\begin{aligned} \mathcal{F}_m^{n(s)}(x)\Big|_{x\to\infty} &= \delta_{nm} k_n^{-1/2} \sin\left[k_n x - \eta_n \ln(2k_n x) + \delta_n\right], \\ \mathcal{F}_m^{n(c)}(x)\Big|_{x\to\infty} &= \delta_{nm} k_n^{-1/2} \cos\left[k_n x - \eta_n \ln(2k_n x) + \delta_n\right], \end{aligned} \tag{A31}$$

where

$$\eta_n = Z/k_n, \qquad \delta_n = \arg\Gamma(1 + i\eta_n). \tag{A32}$$

For closed channels, $k_n^2 < 0$, only irregular solution is needed. It is defined by

$$\mathcal{F}_m^{n(c)}(x)\big|_{x\to\infty} = \delta_{nm} \kappa_n^{-1/2} \exp\left[-\kappa_n x + (Z/\kappa_n) \ln(2\kappa_n x)\right], \tag{A33}$$

where $\kappa_n = |k_n|$. In the main text, these functions are denoted by $\mathcal{F}_m^{n(s,c)}(x; N, Z, k^2, \Lambda, A)$. They can be obtained in the form of asymptotic expansions [8, 9]. In CTBC they are calculated using CPC library subroutine GAILIT [10].

APPENDIX B: DISCRETE VARIABLE REPRESENTATIONS (DVR) BASED ON CLASSICAL ORTHOGONAL POLYNOMIALS (COP)

All numerical schemes used in CTBC are based on DVR. This method was originally proposed in [11], its rigorous mathematical justification was given in [12], but its present wide applications to the numerical solution of various problems in quantum mechanics were initiated in [13], where the method received its name. So far DVR does not belong to the family of traditional numerical methods whose description can be found in standard textbooks on computational mathematics. Rather, it is still in a state of development which can be seen from a large number of publications suggesting new variants of its implementation and generalizations. Here, partly following [14], we describe a well-established and very efficient approach based on COP. All necessary information on COP and associated with them Gaussian quadratures is given in [15]; more thorough discussion of the theory of COP can be found in [16].

1. DVR basis

There are three major types of COP named after Jacobi, Laguerre, and Hermite; all other sets of COP often used in the literature are their particular cases. COP

$$p_n(x), \qquad n = 0, 1, 2, \ldots, \tag{B1}$$

as well as more general sets of orthogonal polynomials, apart from a normalization factor are completely defined by their interval of orthogonality $[a, b]$ and weight function $w(x)$, see table IV. The orthogonality condition reads

$$\int_a^b p_n(x) p_m(x) w(x)\, dx = h_n \delta_{nm}, \tag{B2}$$

where the normalization constant h_n is determined by the convention of standardization. Instead of polynomials (B1) it is more convenient to introduce functions

$$\varphi_n(x) = \sqrt{w(x)/h_{n-1}}\, p_{n-1}(x), \qquad n = 1, 2, 3, \ldots, \tag{B3}$$

which are orthogonal over the same interval with the weight 1 and normalized to 1,

$$\int_a^b \varphi_n(x) \varphi_m(x)\, dx = \delta_{nm}. \tag{B4}$$

TABLE IV: Summary of notations used in Eqs. (B1)-(B6) for three major types of COP.

	Jacobi	Laguerre	Hermite
$p_n(x)$	$P_n^{(\alpha,\beta)}(x)$	$L_n^{(\alpha)}(x)$	$H_n(x)$
$[a,b]$	$[-1,+1]$	$[0,+\infty]$	$[-\infty,+\infty]$
$w(x)$	$(1-x)^\alpha(1+x)^\beta$	$x^\alpha e^{-x}$	e^{-x^2}
$\sigma(x)$	$1-x^2$	x	1
$v(x)$	$\frac{\alpha^2}{2}\frac{1}{1-x}+\frac{\beta^2}{2}\frac{1}{1+x}$	$\frac{1}{4}x+\frac{\alpha^2}{4x}$	x^2
ϵ_n	$(n-1)(n+\alpha+\beta)+\frac{1}{4}(\alpha+\beta)(\alpha+\beta+2)$	$n+\frac{1}{2}(\alpha-1)$	$2n-1$
α_n	$\frac{2}{2n+\alpha+\beta}\sqrt{\frac{n(n+\alpha)(n+\beta)(n+\alpha+\beta)}{(2n+\alpha+\beta)^2-1}}$	$-\sqrt{n(n+\alpha)}$	$\sqrt{n/2}$
β_n	$\frac{\beta^2-\alpha^2}{(2n+\alpha+\beta-2)(2n+\alpha+\beta)}$	$2n+\alpha-1$	0
$\tilde{\alpha}_n$	$-\frac{2n+\alpha+\beta-2}{2n+\alpha+\beta}\sqrt{\frac{n(n+\alpha)(n+\beta)(n+\alpha+\beta)}{(2n+\alpha+\beta)^2-1}}$	$\frac{1}{2}\sqrt{n(n+\alpha)}$	$-\sqrt{n/2}$
$\tilde{\beta}_n$	β_n	$-1/2$	0
$\tilde{\gamma}_n$	$2\alpha_{n-1}-\tilde{\alpha}_{n-1}$	$-\tilde{\alpha}_{n-1}$	$-\tilde{\alpha}_{n-1}$

COP are the solutions of certain EVP formulated on the basis of the hypergeometric equation. As a consequence, functions (B3) satisfy the following *basic* EVP

$$\left[\frac{d}{dx}\sigma(x)\frac{d}{dx}-v(x)+\epsilon_n\right]\varphi_n(x)=0, \tag{B5a}$$

$$\varphi_n(a)<\infty, \quad \varphi_n(b)<\infty, \tag{B5b}$$

where the boundary conditions mean that the solutions are regular at the ends of the interval $a\le x\le b$. Besides, COP satisfy certain three-term recursion relations, which leads to the following properties of functions (B3)

$$x\varphi_n(x)=\alpha_n\varphi_{n+1}(x)+\beta_n\varphi_n(x)+\alpha_{n-1}\varphi_{n-1}(x), \tag{B6a}$$

$$\sigma(x)\frac{d\varphi_n(x)}{dx}=\tilde{\alpha}_n\varphi_{n+1}(x)+\tilde{\beta}_n\varphi_n(x)+\tilde{\gamma}_n\varphi_{n-1}(x). \tag{B6b}$$

All notations here are defined in table IV. For each type of COP there is an associate Gaussian quadrature. An N-point quadrature formula reads

$$\int_a^b F(x)w(x)\,dx\approx\sum_{i=1}^{N}\omega_i F(x_i), \tag{B7}$$

where $F(x)$ is an arbitrary function such that the integral exists, x_i are the quadrature points coinciding with the zeros of $p_N(x)$, and ω_i are the quadrature weights (the Christoffel numbers) given by

$$\omega_i = \frac{k_N h_{N-1}}{k_{N-1} p'_N(x_i) p_{N-1}(x_i)}, \qquad p_n(x) = k_n x^n + \dots \tag{B8}$$

Formula (B7) gives an exact result if $F(x)$ is a polynomial of the degree not higher than $2N-1$, otherwise it is an approximation. Simple and efficient algorithms for the computation of quadrature points x_i and weights ω_i for all three types of COP are described in [17].

Functions (B3), being the solutions of a Sturm-Liouville problem (B5), constitute a complete set in $L_2[a,b]$. Consider an N-dimensional subspace $L_2^{(N)}[a,b]$ of functions

$$\psi^{(N)}(x) = \sqrt{w(x)}\, \mathsf{P}_{N-1}(x), \tag{B9}$$

where $\mathsf{P}_{N-1}(x)$ is an arbitrary polynomial of the degree not higher than $N-1$. Functions

$$\varphi_1(x),\ \varphi_2(x), \dots, \varphi_n(x), \dots, \varphi_N(x) \tag{B10}$$

belong to $L_2^{(N)}[a,b]$ and provide an orthonormal basis there. Thus an arbitrary function from $L_2^{(N)}[a,b]$ can be expanded as

$$\psi^{(N)}(x) = \sum_{n=1}^{N} c_n^{(\varphi)} \varphi_n(x), \qquad c_n^{(\varphi)} = \int_a^b \varphi_n(x) \psi^{(N)}(x)\, dx. \tag{B11}$$

Let us introduce another basis in $L_2^{(N)}[a,b]$,

$$\pi_1(x),\ \pi_2(x), \dots, \pi_i(x), \dots, \pi_N(x). \tag{B12}$$

The two sets (B10) and (B12) are related by

$$\varphi_n(x) = \sum_{i=1}^{N} T_{ni} \pi_i(x), \qquad \pi_i(x) = \sum_{n=1}^{N} T_{ni} \varphi_n(x), \tag{B13}$$

where

$$T_{ni} = (T^{-1})_{in} = \kappa_i \varphi_n(x_i), \qquad \kappa_i \equiv \sqrt{\frac{\omega_i}{w(x_i)}}, \tag{B14}$$

and orthogonality of the transformation matrix T follows from the Christoffel-Darboux identity. It is easy to see that functions $\pi_i(x)$ have the property

$$\pi_i(x_j) = \kappa_i^{-1} \delta_{ij}. \tag{B15}$$

Basis (B12) is also orthonormal,

$$\int_a^b \pi_i(x)\pi_j(x)\,dx = \delta_{ij}, \tag{B16}$$

and an arbitrary function from $L_2^{(N)}[a,b]$ can be expanded as

$$\psi^{(N)}(x) = \sum_{i=1}^{N} c_i^{(\pi)}\pi_i(x), \qquad c_i^{(\pi)} = \int_a^b \pi_i(x)\psi^{(N)}(x)\,dx. \tag{B17}$$

Note that a product of any two functions from $L_2^{(N)}[a,b]$ has a form of the integrand in Eq. (B7), where $F(x)$ is a polynomial of the degree not higher than $2N-2$, hence the quadrature gives an exact result in this case. In particular, it gives an exact result for the normalization integrals (B4) and (B16) within the sets (B10) and (B12) as well as for the integrals defining the coefficients in expansions (B11) and (B17). Using this circumstance and property (B15) we obtain

$$c_i^{(\pi)} = \kappa_i\psi^{(N)}(x_i), \tag{B18}$$

thus the coefficients in (B17) are proportional to the values of $\psi^{(N)}(x)$ at the quadrature points x_i, which is a remarkable property of this expansion. Moreover, Eq. (B7) gives an exact result also for the integrals of a product of any two functions from $L_2^{(N)}[a,b]$ and a polynomial of the first degree, hence

$$\int_a^b \pi_i(x)x\pi_j(x)\,dx = x_i\delta_{ij}. \tag{B19}$$

This result shows that functions (B12) are the basis of a discrete variable representation conjugate to the polynomial basis (B10). For an arbitrary function $f(x)$, using Eqs. (B7) and (B15) we obtain

$$\int_a^b \pi_i(x)f(x)\pi_j(x)\,dx \approx f(x_i)\delta_{ij}. \tag{B20}$$

The smoother is $f(x)$, i.e., the better it can be approximated by a polynomial of low degree, the more accurate is this formula.

2. Application of DVR to the solution of a Sturm-Liouville problem

Many problems in quantum mechanics require to solve the Sturm-Liouville problem

$$\left[\frac{d}{dX}S(X)\frac{d}{dX} + ER(X) - V(X)\right]\Psi(X) = 0 \tag{B21}$$

with appropriate boundary conditions at the ends of the interval $A \le X \le B$, where E and $\Psi(X)$ are the eigenvalue and eigenfunction to be found, and $S(X) \ge 0$, $R(X) \ge 0$, and $V(X)$ are some given functions. Let us introduce a new independent variable x and a new unknown function $\psi(x)$ related to X and $\Psi(X)$ by the transformation

$$X = X(x), \quad \frac{dX(x)}{dx} = f(x) \ge 0, \quad X(a) = A, \; X(b) = B, \tag{B22a}$$

$$\Psi(X) = \Psi(X(x)) = g(x)\psi(x), \tag{B22b}$$

defined by two functions, $f(x)$ and $g(x)$. Substituting Eqs. (B22) into Eq. (B21), the original Sturm-Liouville problem takes the following *standard* form

$$\left[\frac{d}{dx}\sigma(x)\frac{d}{dx} - v(x) - u(x) + E\rho(x)\right]\psi(x) = 0, \tag{B23a}$$

$$\psi(a) < \infty, \qquad \psi(b) < \infty, \tag{B23b}$$

where

$$\sigma(x) = \frac{S(X(x))g^2(x)}{f(x)}, \tag{B24a}$$

$$u(x) = f(x)g^2(x)V(X(x)) - g(x)\frac{d}{dx}\frac{S(X(x))}{f(x)}\frac{d}{dx}g(x) - v(x), \tag{B24b}$$

$$\rho(x) = f(x)g^2(x)R(X(x)). \tag{B24c}$$

We wish to make Eq. (B23) as close in form to the basic EVP (B5) as possible. To this end, we require that the interval $[a, b]$ and functions $\sigma(x)$ and $v(x)$ coincide with the corresponding characteristics for a suitable set of COP, see table IV. Then Eq. (B24a) defines $g(x)$ in terms of $f(x)$. The latter function remains undefined; some recommendations concerning its choice will be given below.

Let us seek an approximate solution of Eq. (B23) by the variational method with trial functions from $L_2^{(N)}[a, b]$,

$$E \approx E^{(N)}, \qquad \psi(x) \approx \psi^{(N)}(x) \in L_2^{(N)}[a, b]. \tag{B25}$$

Because the set (B3) is complete in $L_2[a, b]$, this approximation converges to the exact solution as N grows. Any of the expansions (B11) and (B17) can be used in the variational procedure. Substituting (B11) into Eq. (B23) and using Eq. (B5) we obtain a generalized algebraic EVP in the φ representation,

$$\left(\boldsymbol{\epsilon}^{(\varphi)} + \mathbf{u}^{(\varphi)}\right) c^{(\varphi)} = E^{(N)}\boldsymbol{\rho}^{(\varphi)}c^{(\varphi)}, \tag{B26}$$

where

$$\boldsymbol{\epsilon}^{(\varphi)}_{nm} = \epsilon_n \delta_{nm}, \tag{B27a}$$

$$\mathbf{u}^{(\varphi)}_{nm} = \int_a^b \varphi_n(x) u(x) \varphi_m(x)\, dx, \tag{B27b}$$

$$\boldsymbol{\rho}^{(\varphi)}_{nm} = \int_a^b \varphi_n(x) \rho(x) \varphi_m(x)\, dx. \tag{B27c}$$

Starting from (B17) and acting similarly we obtain a generalized algebraic EVP in the π representation,

$$\left(\boldsymbol{\epsilon}^{(\pi)} + \mathbf{u}^{(\pi)}\right) c^{(\pi)} = E^{(N)} \boldsymbol{\rho}^{(\pi)} c^{(\pi)}, \tag{B28}$$

where

$$\boldsymbol{\epsilon}^{(\pi)}_{ij} = \sum_{n=1}^{N} T_{ni} \epsilon_n T_{nj}, \tag{B29a}$$

$$\mathbf{u}^{(\pi)}_{ij} = \int_a^b \pi_i(x) u(x) \pi_j(x)\, dx, \tag{B29b}$$

$$\boldsymbol{\rho}^{(\pi)}_{ij} = \int_a^b \pi_i(x) \rho(x) \pi_j(x)\, dx. \tag{B29c}$$

If all the integrals defining matrices $\mathbf{u}$ and $\boldsymbol{\rho}$ in Eqs. (B26) and (B28) were calculated exactly, these equations would be related by the orthogonal transformation (B14) and both approaches would obviously yield identical results. The essence of DVR is to calculate matrices $\mathbf{u}$ and $\boldsymbol{\rho}$ approximately using the quadrature (B7). In this case it is more convenient to work in the π representation. From Eq. (B20) we obtain

$$\mathbf{u}^{(\pi)}_{ij} \approx u(x_i)\delta_{ij}, \tag{B30a}$$

$$\boldsymbol{\rho}^{(\pi)}_{ij} \approx \rho(x_i)\delta_{ij}. \tag{B30b}$$

Seeking an approximate solution of Eq. (B23) in the form

$$E \approx E^{(\mathrm{DVR})}, \qquad \psi(x) \approx \psi^{(\mathrm{DVR})}(x) = \sum_{i=1}^{N} \frac{c_i^{(\mathrm{DVR})}}{\sqrt{\rho(x_i)}} \pi_i(x), \tag{B31}$$

and using Eqs. (B30), we obtain an ordinary algebraic EVP,

$$\mathbf{h}^{(\mathrm{DVR})} c^{(\mathrm{DVR})} = E^{(\mathrm{DVR})} c^{(\mathrm{DVR})}, \tag{B32}$$

where

$$\mathbf{h}^{(\mathrm{DVR})}_{ij} = \frac{\boldsymbol{\epsilon}^{(\pi)}_{ij}}{\sqrt{\rho(x_i)\rho(x_j)}} + \frac{u(x_i)}{\rho(x_i)} \delta_{ij}. \tag{B33}$$

This is the DVR. Due to property (B15), the components of the eigenvectors $c^{(\mathrm{DVR})}$ are proportional to the values of the corresponding eigenfunctions at the quadrature points,

$$\psi(x_i) \approx \sqrt{\frac{w(x_i)}{\omega_i \rho(x_i)}}\, c_i^{(\mathrm{DVR})}. \tag{B34}$$

The values of $\psi(x)$ at an arbitrary point of the interval $[a, b]$ can be obtained by transforming expansion (B31) back to the polynomial basis (B10).

As can be seen from the above discussion, DVR contains an additional approximation (B30) in comparison with the variational method. The accuracy of this approximation depends on functions $u(x)$ and $\rho(x)$. If these functions are linear, then formulas (B30) are exact, and the variational (B25) and DVR (B31) solutions coincide. Otherwise they are different, however, the difference is the smaller the better $u(x)$ and $\rho(x)$ can be approximated by polynomials of low degree. This circumstance should serve as a guide in choosing the function $f(x)$ defining the transformation (B22) of the original Sturm-Liouville problem (B21) to the standard form (B23), the other function $g(x)$ in this transformation being determined by Eq. (B24a). The present approach does not provide a unique prescription for $f(x)$, but in each case a suitable function can be usually found without difficulties. It should be noted that if the transformation of the independent variable in (B22) is linear, i.e., $f(x)$ is a constant, then the type of COP used for constructing the DVR and all the other parts of the described scheme are defined uniquely. If functions $u(x)$ and $\rho(x)$ are sufficiently smooth, the difference between the variational and DVR solutions is small, and then in choosing between the two methods one should consider the matters of simplicity in implementation and convenience in practical calculations. Here DVR has several important advantages. First, for calculating the DVR Hamiltonian (B33) one needs to know only the values of $u(x)$ and $\rho(x)$ at the quadrature points x_i. Second, matrix $\boldsymbol{\epsilon}^{(\pi)}$ depends only on the type of COP and the dimension of the basis N and does not depend on the particular problem under consideration, therefore it should be calculated once and then can be used for recurrent solution of the same problem with different values of some parameters defining the functions $\rho(x)$ and $u(x)$. Finally, the form of the DVR solution (B31) is very convenient for subsequent calculations of various matrix elements using Eq. (B20).

3. Application of DVR in the SVD method

A general scheme of the SVD method [3] requires to calculate matrices of the kinetic energy operator and weight function in a suitable DVR basis. In the applications of SVD to the solution of the three-body Coulomb problem in hyperspherical coordinates these matrices can be calculated analytically. Here we summarize the results used in CTBC.

a. Kinetic matrix for bound states

For bound states, the DVR basis is constructed from Laguerre polynomials $L_n^{(\alpha)}(x)$. The kinetic matrix (97) in this case is given by

$$K_{ij} = \frac{1}{2}\int_0^\infty \frac{d\pi_i(x)}{dx}\, x^2\, \frac{d\pi_j(x)}{dx}\, dx = \sum_{n,m=1}^{N} T_{ni} K^{(\varphi)}_{nm} T_{mj}, \tag{B35}$$

where

$$K^{(\varphi)}_{nm} = \frac{1}{2}\int_0^\infty \frac{d\varphi_n(x)}{dx}\, x^2\, \frac{d\varphi_m(x)}{dx}\, dx. \tag{B36}$$

This is a symmetric matrix with three nonzero diagonals,

$$\begin{aligned} K^{(\varphi)}_{nn} &= \tfrac{1}{8}\left[2n^2 + 2(\alpha-1)n - \alpha + 2\right], \\ K^{(\varphi)}_{n\,n+2} &= K^{(\varphi)}_{n+2\,n} = -\tfrac{1}{8}\left[n(n+1)(n+\alpha)(n+\alpha+1)\right]^{1/2}. \end{aligned} \tag{B37}$$

Matrix (B35) is calculated by subroutine DVRB.

b. Kinetic matrix for scattering in the first sector

For scattering in the first sector, the DVR basis is constructed from Jacobi polynomials $P_n^{(0,\beta)}(x)$. The kinetic matrix (97) in this case is given by

$$K_{ij} = \frac{1}{2}\int_{-1}^{1} \frac{d\pi_i(x)}{dx}\, (1+x)^2\, \frac{d\pi_j(x)}{dx}\, dx = \sum_{n,m=1}^{N} T_{ni} K^{(\varphi)}_{nm} T_{mj}, \tag{B38}$$

where

$$K^{(\varphi)}_{nm} = \frac{1}{2}\int_{-1}^{1} \frac{d\varphi_n(x)}{dx}\, (1+x)^2\, \frac{d\varphi_m(x)}{dx}\, dx. \tag{B39}$$

We have

$$(1+x)\,\frac{d\varphi_n(x)}{dx} = \sum_{k=1}^{n} a_{nk}\varphi_k(x), \tag{B40}$$

where

$$a_{nk} = \int_{-1}^{1} \varphi_k(x)(1+x)\,\frac{d\varphi_n(x)}{dx}\,dx. \tag{B41}$$

Using

$$\int_{-1}^{1} \frac{d}{dx}\left[\varphi_n(x)(1+x)\varphi_k(x)\right]\,dx = a_{nk} + a_{kn} + \delta_{nk} = 2\varphi_n(1)\varphi_k(1), \tag{B42}$$

we find

$$\begin{aligned} a_{nn} &= \varphi_n^2(1) - \tfrac{1}{2}, \\ a_{nk} &= 2\varphi_n(1)\varphi_k(1), \quad k < n. \end{aligned} \tag{B43}$$

From this we obtain

$$\begin{aligned} K_{nn}^{(\varphi)} &= 2\varphi_n^2(1)\sum_{k=1}^{n-1}\varphi_k^2(1) + \tfrac{1}{2}\left[\varphi_n^2(1) - \tfrac{1}{2}\right]^2, \\ K_{nm}^{(\varphi)} &= K_{mn}^{(\varphi)} = \varphi_n(1)\varphi_m(1)\left[2\sum_{k=1}^{n-1}\varphi_k^2(1) + \varphi_n^2(1) - \tfrac{1}{2}\right], \quad n < m. \end{aligned} \tag{B44}$$

Matrix (B38) is calculated by subroutine DVRSJ.

c. Kinetic matrix for scattering in further sectors

For scattering in all further sectors, the DVR basis is constructed from Legendre polynomials $P_n(x)$. The kinetic matrix (97) in this case has the form

$$K_{ij} = c_0 k_{ij}^{(0)} + c_1 k_{ij}^{(1)} + c_2 k_{ij}^{(2)}, \qquad k_{ij}^{(l)} = \int_{-1}^{1} \frac{d\pi_i(x)}{dx}\,x^l\,\frac{d\pi_j(x)}{dx}\,dx. \tag{B45}$$

We have

$$\frac{d\varphi_n(x)}{dx} = \sum_{k=1}^{n-1} a_{nk}\varphi_k(x), \tag{B46}$$

where

$$a_{nk} = \int_{-1}^{1} \varphi_k(x)\frac{d\varphi_n(x)}{dx}\,dx. \tag{B47}$$

From

$$\int_{-1}^{1} \frac{d}{dx}\left[\varphi_n(x)\varphi_k(x)\right]\,dx = a_{nk} + a_{kn} = \tfrac{1}{2}\sqrt{(2n-1)(2k-1)}\left(1 - (-1)^{n+k}\right) \tag{B48}$$

we find

$$a_{nk} = \begin{cases} \sqrt{(2n-1)(2k-1)}, & \text{if } k = n-1, n-3, \ldots \geq 1, \\ 0, & \text{otherwise.} \end{cases} \tag{B49}$$

Using this we obtain

$$k_{ij}^{(0)} = \sum_{n,m=1}^{N} T_{ni} T_{mj} \int_{-1}^{1} \frac{d\varphi_n(x)}{dx} \frac{d\varphi_m(x)}{dx}\, dx = \sum_{k=1}^{N} b_{ik} b_{jk}, \tag{B50}$$

where

$$b_{ik} = \sum_{n=1}^{N} T_{ni} a_{nk}. \tag{B51}$$

Next

$$k_{ij}^{(1)} = \sum_{n,m=1}^{N} T_{ni} T_{mj} \int_{-1}^{1} \frac{d\varphi_n(x)}{dx}\, x\, \frac{d\varphi_m(x)}{dx}\, dx = \sum_{k=1}^{N-1} \frac{k}{\sqrt{4k^2-1}} \left(b_{ik} b_{jk+1} + b_{ik+1} b_{jk} \right), \tag{B52}$$

and finally

$$k_{ij}^{(2)} = k_{ij}^{(0)} - \sum_{n=1}^{N} (n-1) n T_{ni} T_{nj}. \tag{B53}$$

Matrices $k_{ij}^{(l)}$ in (B45) are calculated by subroutine DVRSL.

d. Weight matrix

In all the cases considered above, the weight matrix (98) has the form

$$\rho_{ij} = \int \pi_i(x) \rho(x) \pi_j(x)\, dx, \qquad \rho(x) = c_0 + c_1 x + c_2 x^2. \tag{B54}$$

We have

$$\begin{aligned} \int \pi_i(x) x^2 \pi_j(x)\, dx &= \sum_{n,m=1}^{N} T_{ni} T_{mj} \int \varphi_n(x) x^2 \varphi_m(x)\, dx \\ &= \sum_{n,m=1}^{N} T_{ni} T_{mj} \left(\sum_{k=1}^{N} T_{nk} x_k^2 T_{mk} + \Delta(N) \delta_{nN} \delta_{mN} \right) \\ &= x_i^2 \delta_{ij} + \Delta(N) T_{Ni} T_{Nj}, \end{aligned} \tag{B55}$$

and therefore

$$\rho_{ij} = \rho(x_i) \delta_{ij} + c_2 \Delta(N) T_{Ni} T_{Nj}, \tag{B56}$$

where

$$\Delta(N) = \int \varphi_N(x) x^2 \varphi_N(x)\, dx - \sum_{k=1}^{N} T_{Nk} x_k^2 T_{Nk}. \tag{B57}$$

It remains to calculate $\Delta(N)$. First,

$$\int \varphi_N(x) x^2 \varphi_N(x)\, dx = \alpha_N^2 + \beta_N^2 + \alpha_{N-1}^2. \tag{B58}$$

Second, taking into account that $T_{N+1\,i} = 0$,

$$x_i T_{Ni} = \beta_N T_{Ni} + \alpha_{N-1} T_{N-1\,i}. \tag{B59}$$

From this using the orthogonality of T we obtain

$$\sum_{k=1}^{N} T_{Nk} x_k^2 T_{Nk} = \beta_N^2 + \alpha_{N-1}^2. \tag{B60}$$

Thus $\Delta(N) = \alpha_N^2$. In the cases of interest here

$$\Delta(N) = \begin{cases} N(N+\alpha), & \text{for } L_n^{(\alpha)}(x), \\ \dfrac{4N^2(N+\beta)^2}{(2N+\beta)^2[(2N+\beta)^2-1]}, & \text{for } P_n^{(0,\beta)}(x), \\ \dfrac{N^2}{4N^2-1}, & \text{for } P_n(x). \end{cases} \tag{B61}$$

REFERENCES

[1] R. G. Newton, *Scattering Theory of Waves and Particles* (Springer-Verlag, New York, 1982).

[2] J. Macek, J. Phys. B **1**, 831 (1968).

[3] O. I. Tolstikhin, S. Watanabe, and M. Matsuzawa, J. Phys. B **29**, L389 (1996).

[4] C. Bloch, Nucl. Phys. **4**, 503 (1957).

[5] D. Kato and S. Watanabe, Phys. Rev. A **56**, 3687 (1997).

[6] E. P. Wigner and L. Eisenbud, Phys. Rev. **72**, 29 (1947).

[7] K. L. Baluja, P. G. Burke, and L. A. Morgan, Comp. Phys. Comm. **27**, 299 (1982).

[8] P. G. Burke and H. M. Schey, Phys. Rev. **126**, 147 (1962).

[9] M. Gailitis, J. Phys. B **9**, 843 (1976).

[10] C. J. Noble and R. K. Nesbet, Comput. Phys. Commun. **33**, 399 (1984).

[11] D. O. Harris, G. G. Engerholm, W. D. Gwinn, J. Chem. Phys. **43**, 1515 (1965).

[12] A. S. Dickinson, P. R. Certain, J. Chem. Phys. **49**, 4209 (1968).

[13] J. C. Light, I. P. Hamilton, J. V. Lill, J. Chem. Phys. **82**, 1400 (1985).

[14] O. I. Tolstikhin, D. Kato, T. Morishita, S. Watanabe, and M. Matsuzawa, unpublished (1995).

[15] *Handbook of Mathematical Functions*, edited by M. Abramowitz and I. A. Stegun (Dover Publications Inc., New York, 1972).

[16] A. F. Nikiforov and V. B. Uvarov, *Special Functions of Mathematical Physics* (Birkhäuser Verlag, Basel, 1988).

[17] W. H. Press, S. A. Teukolsky, W. T. Vetterling, and B. P. Flannery, *Numerical Recipes in FORTRAN* (Cambridge University Press, Cambridge, 1992).

Recent Issues of NIFS Series

NIFS-759 S. Kubo, T. Shimozuma, H. Idei, Y. Yoshimura, T. Notake, M. Sato, K. Ohkubo, T. Watari,K. Narihara, I. Yamada, S. Inagaki, Y. Nagayama, S. Murakami, S. Muto,Y. Takeiri, M. Yokoyama, N. Ohyabu, K. Ida, K. Kawahata, O. Kaneko, A. Komori, T. Mutoh, Y. Nakamura, H. Yamada, T. Akiyama, N. Ashikawa, M. Emoto, H. Funaba, P. Goncharov M. Goto, K. Ikeda, M. Isobe, H. Kawazome, K. Khlopenkov, T. Kobuchi, A. Kostrioukov, R. Kumazawa, Y. Liang, S. Masuzaki, T. Minami, J. Miyazawa, T. Morisaki, S. Morita, H. Nakanishi, Y. Narushima, K. Nishimura, N. Noda, H. Nozato, S. Ohdachi, Y. Oka, M. Osakabe, T. Ozaki, B. J. Peterson, A. Sagara, T. Saida, K. Saito, S. Sakakibara, R. Sakamoto, M. Sasao, K. Sato, T. Seki, M. Shoji, H. Suzuki, N. Takeuchi, N. Tamura, K. Tanaka, K. Toi, T. Tokuzawa, Y. Torii, K. Tsumori, K. Y. Watanabe, Y. Xu, S. Yamamoto, T. Yamamoto, M. Yoshinuma, K. Itoh, T. Satow, S. Sudo, T. Uda, K. Yamazaki, K. Matsuoka, O. Motojima, Y. Hamada and M. Fujiwara

Transport Barrier Formation by Application of Localized ECH in the LHD
Oct. 2002 (EX/C4-5Rb)

NIFS-760 T. Hayashi, N. Mizuguchi, H. Miura, R. Kanno, N. Nakajima and M. Okamoto
Nonlinear MHD Simulations of Spherical Tokamak and Helical Plasmas
Oct. 2002 (TH/6-3)

NIFS-761 K. Yamazaki, S. Imagawa, T. Muroga, A. Sagara, S. Okamura
System Assessment of Helical Reactors in Comparison with Tokamaks
Oct. 2002 (FT/P1-20)

NIFS-762 S. Okamura, K. Matsuoka, S. Nishimura, M. Isobe, C. Suzuki, A. Shimizu, K. Ida, A. Fujisawa, S. Murakami, M. Yokoyama, K. Itoh, T. Hayashi, N. Nakajima, H. Sugama, M. Wakatani, Y. Nakamura, W. Anthony Cooper
Physics Design of Quasi-Axisymmetric Stellarator CHS-qa
Oct. 2002 (IC/P-07)

NIFS-763 Lj. Nikolic, M.M. Skoric, S. Ishiguro and T. Sato
On Stimulated Scattering of Laser Light in Inertial Fusion Energy Targets
Nov. 2002

NIFS-764
NIFS Contributions to 19th IAEA Fusion Energy Conference (Lyon, France, 14-19 October 2002)
Nov. 2002

NIFS-765 S. Goto and S. Kida
Enhanced Stretching of Material Lines by Antiparallel Vortex Pairs in Turbulence
Dec. 2002

NIFS-766 M. Okamoto, A.A. Maluckov, S. Satake, N. Nakajima and H. Sugama
Transport and Radial Electric Field in Torus Plasmas
Dec. 2002

NIFS-767 R. Kanno, N. Nakajima, M. Okamoto and T. Hayashi
Computational Study of Three Dimensional MHD Equilibrium with m/n=1/1 Island
Dec. 2002

NIFS-768 M. Yagi, S.-I. Itoh, M. Kawasaki, K. Itoh and A. Fukuyama
Multiple-Scale Turbulence and Bifurcaion
Jan. 2003

NIFS-769 S.-I. Itoh, K. Itoh and S. Toda
Statistical Theory of L-H Transition and its Implication to Threshold Database
Jan. 2003

NIFS-770 K. Itoh
Summary: Theory of Magnetic Confinement
Jan. 2003

NIFS-771 S.-I. Itoh, K. Itoh and S. Toda
Statistical Theory of L-H Transition in Tokamaks
Jan. 2003

NIFS-772 M. Stepic, L. Hadzievski and M.M. Skoric
Modulation Instability in Two-dimensional Nonlinear Schrodinger Lattice Models with Dispersion and Long-range Interactions
Jan. 2003

NIFS-773 M.Yu. Isaev, K.Y. Watanabe, M. Yokoyama and K. Yamazaki
The Effect of Hexapole and Vertical Fields on α-particle Confinement in Heliotron Configurations
Mar. 2003

NIFS-774 K. Itoh, S.-I. Itoh, F. Spineanu, M.O. Vlad and M. Kawasaki
On Transition in Plasma Turbulence with Multiple Scale Lengths
May 2003

NIFS-775 M. Vlad, F. Spineanu, K. Itoh, S.-I. Itoh
Intermittent and Global Transitions in Plasma Turbulence
July 2003

NIFS-776 Y. Kondoh, M. Kondo, K. Shimoda, T. Takahashi and K. Osuga
Innovative Direct Energy Conversion Systems from Fusion Output Thermal Power to the Electrical One with the Use of Electronic Adiabatic Processes of Electron Fluid in Solid Conductors.
July 2003

NIFS-777 S.-I. Itoh, K. Itoh and M. Yagi
A Novel Turbulence Trigger for Neoclassical Tearing Modes in Tokamaks
July 2003

NIFS-778 T. Utsumi, J. Koga, T. Yabe, Y. Ogata, E. Matsunaga, T. Aoki and M. Sekine
Basis Set Approach in the Constrained Interpolation Profile Method
July 2003

NIFS-779 Oleg I. Tolstikhin and C. Namba
CTBC A Program to Solve the Collinear Three-Body Coulomb Problem: Bound States and Scattering Below the Three-Body Disintegration Threshold
Aug. 2003

Printed on 100% Recycled Paper for this Text